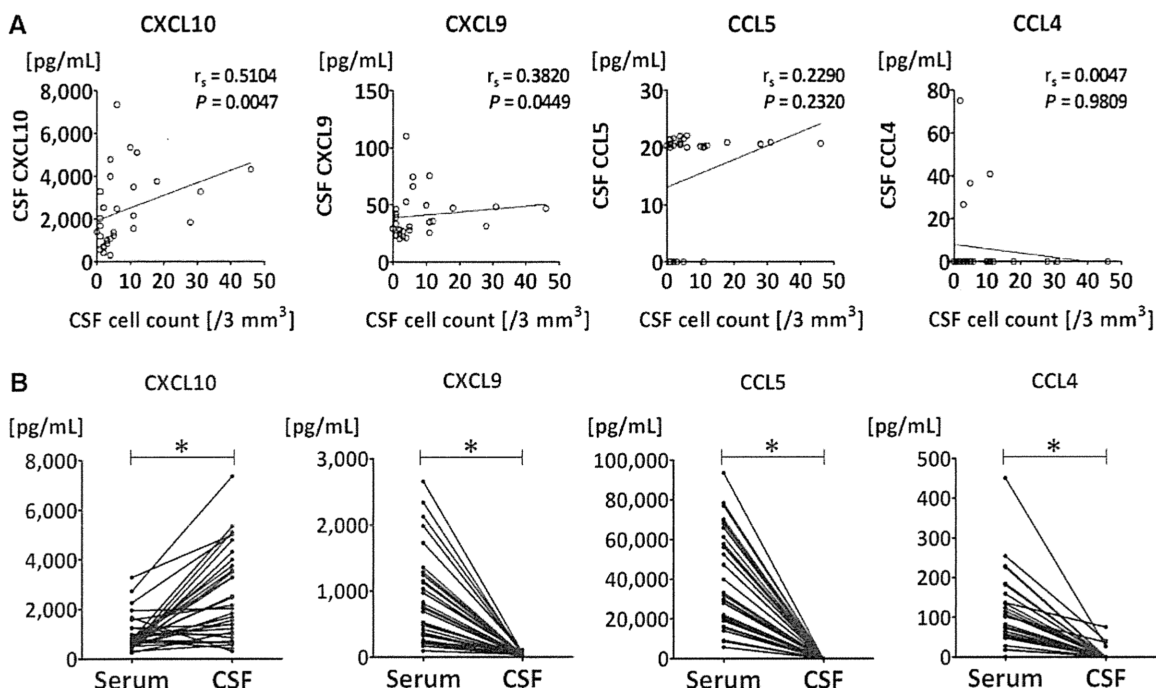

Figure 1 CXCL10 levels in CSF of patients with HAM/TSP were correlated with CSF cell counts and were significantly higher than those in serum of patients with HAM/TSP. (**A**) Correlation analysis between CSF levels of four chemokines (CXCL10, CXCL9, CCL5 and CCL4) and CSF cell counts in patients with HAM/TSP ($n = 29$). Statistical analysis was performed using Spearman's rank test. The linear regression line is indicated by a straight line in each graph. (**B**) Comparison of concentrations of four chemokines (CXCL10, CXCL9, CCL5, and CCL4) in CSF and serum samples obtained from patients with HAM/TSP such that all samples from a given patient were taken within a 1-h window of the first sample taken from that patient ($n = 32$). $^*P < 0.0001$ by the paired t-test.

CXCR3$^+$ cells among CSF cells was $92.4 \pm 7.0\%$, whereas the average percentage of CXCR3$^+$ cells among peripheral blood mononuclear cells was $9.9 \pm 8.2\%$ ($P < 0.0001$, Fig. 2B). Immunofluorescence staining revealed abundant CXCR3$^+$ cell infiltrate around small vessels in the leptomeninges of spinal cord lesions in patients with HAM/TSP (Fig. 2C). We examined the types of CXCR3$^+$ cells in the CSF using flow cytometry and found that CSF CXCR3$^+$ cells mainly consist of CD3$^+$ cells (>90%) and small populations of CD14$^+$ and CD19$^+$ cells (Fig. 2D, left). Uniquely, the percentage of CXCR3$^+$ cells was extremely high in all CSF cell populations under study, especially CD4$^+$ ($94.33 \pm 2.95\%$), CD8$^+$ ($98.64 \pm 1.05\%$), and even CD14$^+$ ($84.97 \pm 18.49\%$) and CD19$^+$ ($76.38 \pm 17.35\%$) cells (Supplementary Fig. 2). Our data show that the ratio of CD4$^+$ to CD8$^+$ cells in the CSF was ~1:1 in patients with HAM/TSP (Fig. 2D, right). In both these cell populations, the rate of CXCR3 positivity was higher in CSF cells than in peripheral blood mononuclear cells (Supplementary Fig. 2). The percentage of CXCR3$^+$ cells in peripheral blood mononuclear cells of patients with HAM/TSP was lower than those in peripheral blood mononuclear cells of asymptomatic carriers as well as healthy donors; however, there were no significant differences between patients with adult T cell leukaemia and patients with HAM/TSP (Supplementary Fig. 3A). This lower percentage of CXCR3$^+$ cells in patients with HAM/TSP was observed even when compared with asymptomatic carriers with equivalently high proviral loads (Supplementary Fig. 3B). Finally, to support our hypothesis that HTLV-1-infected T cells (the majority of which are known to be CD4$^+$) migrate from the circulating blood to the spinal cord tissue through CXCL10–CXCR3 interaction, we confirmed that there does exist a subset of peripheral CD4$^+$CXCR3$^+$ T cells infected with HTLV-1 (Fig. 2E).

Numerous CXCL10-producing cells in inflamed spinal cords of patients with HAM/TSP

To quantitatively compare the level of expression of CXCL10, we microscopically counted the number of CXCL10$^+$ cells in the spinal cord tissue and found a larger number of CXCL10$^+$ cells in the spinal cord lesions of patients with HAM/TSP than in control patients (Fig. 3A, $P = 0.0095$). In addition, we compared tissue sections from the thoracic spinal cord (a region of high inflammation) and the medulla oblongata (comparatively very low inflammation) from a single patient with HAM/TSP, and we observed a much larger CXCL10 presence in the thoracic spinal cord region (Supplementary Fig. 4).

Astrocytes as the main producers of CXCL10 in the spinal cords of patients with HAM/TSP

To identify which cell populations are the main CXCL10 producers, we immunostained thoracic spinal cord tissues from patients with

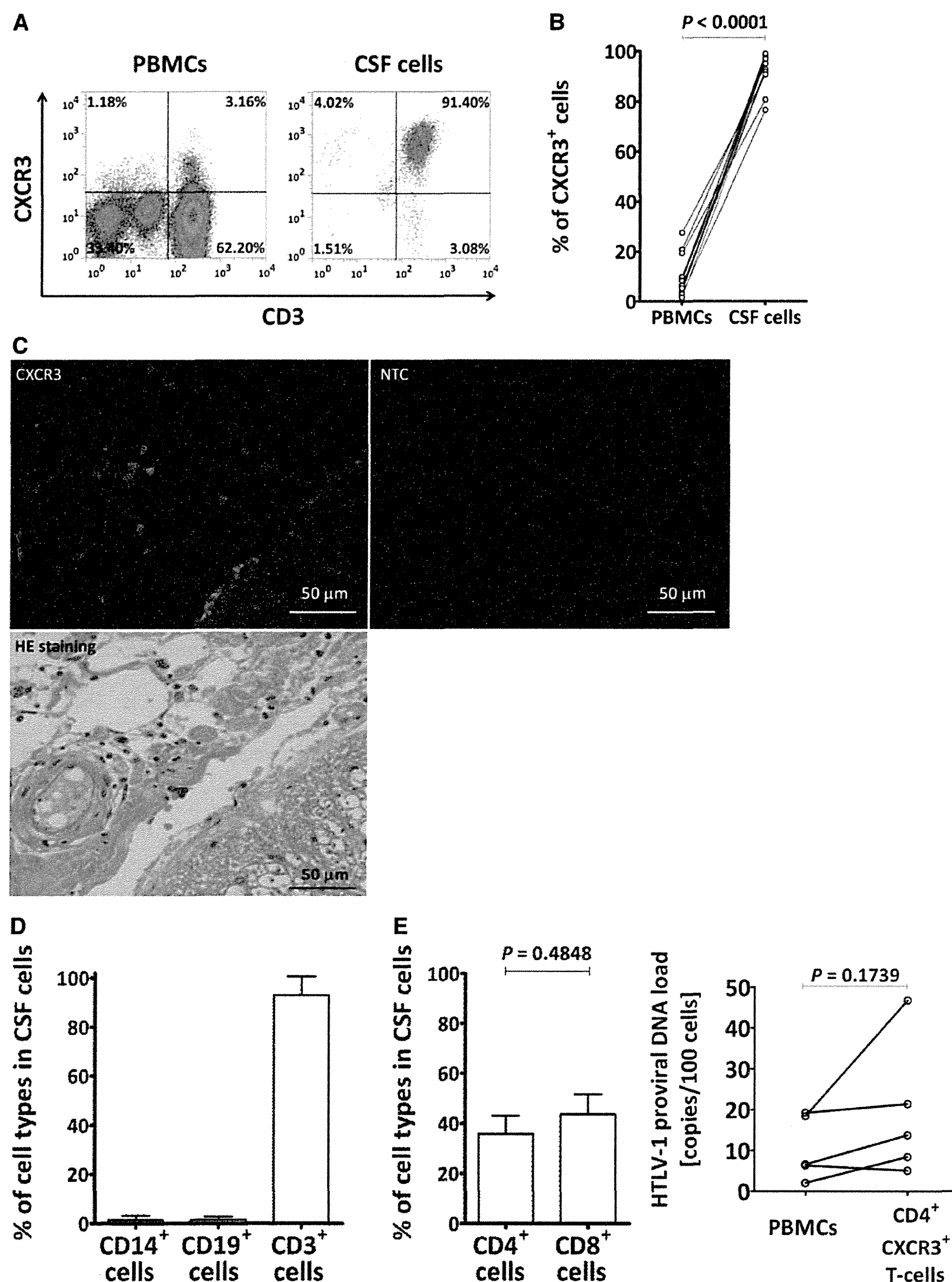

Figure 2 Abundant CXCR3$^+$ cells in the CSF and spinal cord tissue of patients with HAM/TSP. (**A**) Representative dot plots of CD3 and CXCR3 expression in peripheral blood mononuclear cells (PBMCs, *left*) and CSF cells (*right*) from a patient with HAM/TSP measured using flow cytometry. (**B**) Comparison of the percentages of CXCR3$^+$ cells in peripheral blood mononuclear cells and CSF cells, samples of which were obtained from 12 patients with HAM/TSP such that all samples from a given patient were taken within a 1-h window of the first sample taken from that patient. Statistical analysis was performed using the paired *t*-test. See also Supplementary Fig. 2. (**C**) Representative images of immunofluorescent detection of CXCR3, shown in green (*upper* panels), and haematoxylin-eosin (HE) staining for inflammatory cells, shown in blue (*lower* panel), in the thoracic spinal cords of patients with HAM/TSP. Rabbit IgG antibody used as the negative control (NTC). (**D**) *Left*: Percentages of CD3$^+$, CD19$^+$, and CD14$^+$ cells in CSF cells derived from patients with HAM/TSP ($n = 6$). *Right*: Percentages of CD4$^+$ cells and CD8$^+$ cells. Statistical analysis was performed using the Mann–Whitney U-test. Error bars represent the mean ± SD. (**E**) The HTLV-1 proviral DNA loads of CD4$^+$CXCR3$^+$ T cells with peripheral blood mononuclear cells as the control. This result confirms the non-negligible existence of HTLV-1-infected CD4$^+$CXCR3$^+$ T cells, which may migrate to the CNS. Cells are from patients with HAM/TSP ($n = 5$). Statistical analysis was performed using the paired *t*-test.

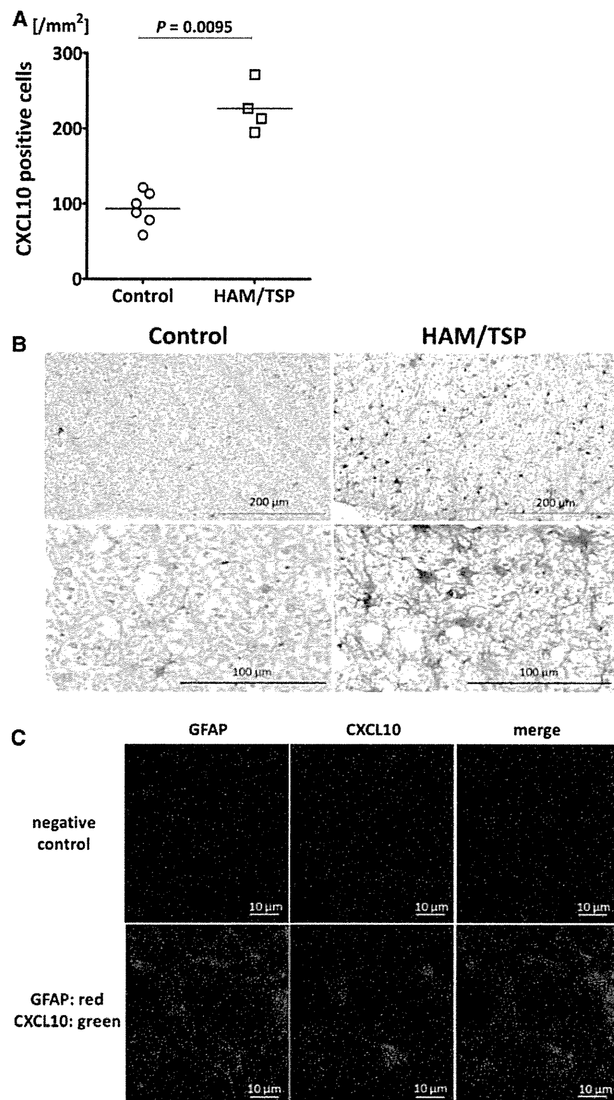

Figure 3 Astrocytes are the major CXCL10-producing cells in the spinal cords of patients with HAM/TSP. (**A**) Quantitative histological analysis (control: $n = 6$, HAM/TSP: $n = 4$). The numbers of CXCL10^{+} cells in the spinal cord sections were counted under a microscope. The data represent the mean number of CXCL10^{+} cells in three random fields of 1 mm^2 per sample. Horizontal bars represent the mean. Statistical analysis was performed using the Mann–Whitney U-test. (**B**) Representative immunohistochemistical images of CXCL10 in the thoracic spinal cord tissues from control individuals ($n = 6$) and patients with HAM/TSP ($n = 4$). CXCL10-positive cells are brown. *Upper* panel: low magnification; *Lower* panel: high magnification. (**C**) Representative immunofluorescent images of GFAP (red), a marker for astrocytes, and CXCL10 (green) in the thoracic spinal cord tissues from a control individual and a patient with HAM/TSP patient. Similar results were observed in images of spinal cord tissues obtained from two other patients with HAM/TSP.

HAM/TSP ($n = 4$) and control individuals ($n = 6$). CXCL10-positive staining was mainly observed in star-shaped cells with extensive and radiating cytoplasmic processes, indicating that CXCL10 is expressed in activated astrocytes in the thoracic spinal cord of patients with HAM/TSP (Fig. 3B). We also used immunofluorescence to confirm that CXCL10 is mainly expressed in astrocytes (GFAP^{+} cells) (Fig. 3C).

Co-culture with CD4^{+} T cells from patients with HAM/TSP enhances CXCL10 production in U251 human astrocytoma cells

CXCL10, also known as an IFN-γ-inducible protein 10, is mainly produced in response to IFN-γ stimulation (Muller *et al.*, 2010). We used this fact to investigate the events leading to CXCL10 production by astrocytes in the spinal cords of patients with HAM/TSP. First, we compared the capacities of several purified cell populations within peripheral blood mononuclear cells to produce IFN-γ spontaneously, i.e. without any stimulation. We found that CD4^{+} T cells exhibited the highest production of IFN-γ among peripheral blood mononuclear cells isolated from patients with HAM/TSP, and CD4^{+} T cells from patients with HAM/TSP produced more IFN-γ than those from asymptomatic carriers (Fig. 4A and B left). No peripheral blood mononuclear cells isolated from healthy donors displayed any detectable level of IFN-γ production (data not shown). Interestingly, CD4^{+} T cells from patients with HAM/TSP did not produce IL-17A, a proinflammatory cytokine known to play a key role in the pathogenic inflammatory response that characterizes multiple sclerosis (Fig. 4B, right) (Matusevicius *et al.*, 1999). Next, we used a co-culture system to confirm that CD4^{+} T cells induce astrocytes to produce CXCL10 by releasing IFN-γ. CD4^{+} T cells from patients with HAM/TSP induced CXCL10 production in U251 astrocytoma cells in a cell number-dependent manner (Fig. 4C), whereas CD4^{+} T cells from healthy donors did not induce CXCL10 production (data not shown). Importantly, in the presence of anti-IFN-γ neutralizing antibodies, the supernatant from HAM/TSP patient CD4^{+} T cell cultures stimulated significantly less CXCL10 production in U251 cells (Fig. 4D).

Chemotaxis of peripheral blood mononuclear cells from patients with HAM/TSP due to CXCL10 and inhibition of chemotaxis by anti-CXCL10 neutralizing antibodies

To investigate the potential role of CXCL10 or CXCR3 as a therapeutic target for inhibiting the migration of proinflammatory cells into the CNS, we assessed whether neutralizing antibodies against CXCL10 or CXCR3 could inhibit the migration of peripheral blood mononuclear cells in patients with HAM/TSP through the use of an *in vitro* chemotaxis assay system. Human CXCL10 increased the chemotactic activity of peripheral blood mononuclear cells from patients with HAM/TSP by ~1.7-fold (Fig. 5A). Compared with isotype control monoclonal antibodies, the chemotactic activity due to CXCL10 was inhibited by anti-CXCL10 neutralizing antibodies (Fig. 5A; 65.9% inhibition, $P < 0.01$) but not by anti-CXCR3 antibodies (Fig. 5A; 9.2% inhibition, $P > 0.05$: not

Downloaded from http://brain.oxfordjournals.org/ at St. Marianna University School of Medicine on July 28, 2013

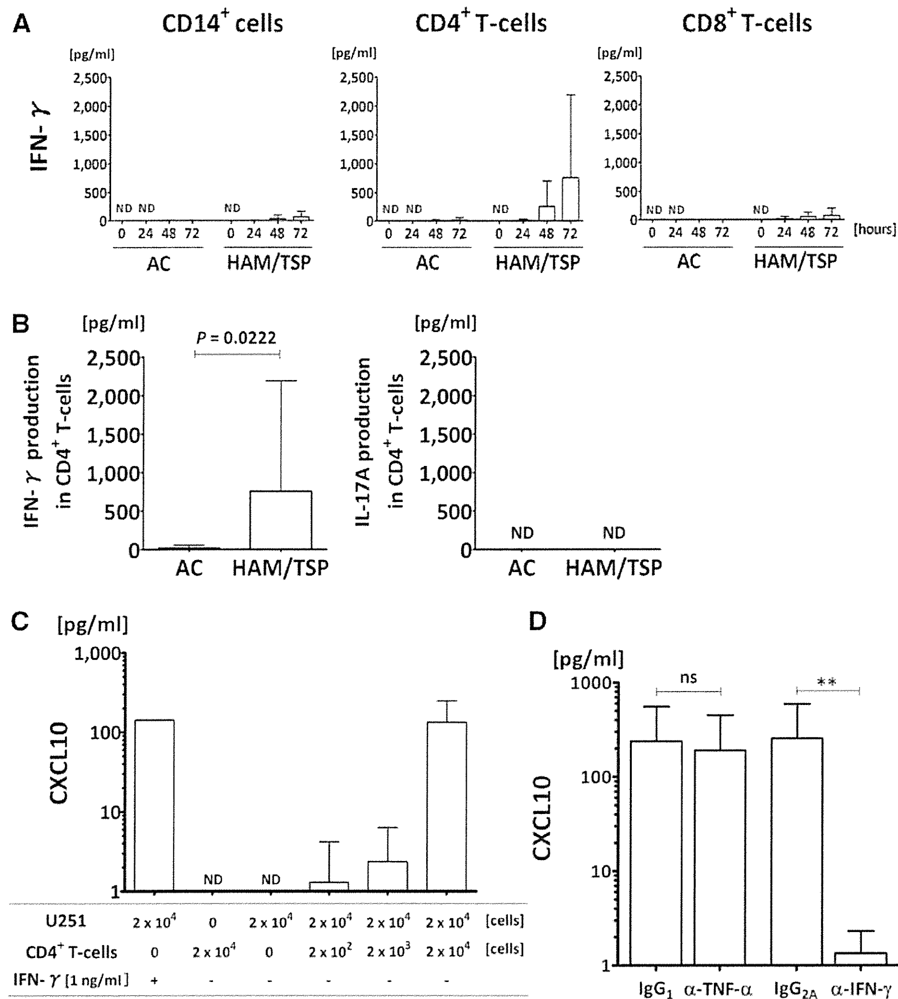

Figure 4 Co-culturing with CD4$^+$ T cells from patients with HAM/TSP increases CXCL10 production in a U251 human astrocytoma cell line. (**A**) Concentration of IFN-γ in supernatants of cultured CD4$^+$, CD8$^+$, or CD14$^+$ cells in peripheral blood mononuclear cells (PBMCs) from patients with HAM/TSP (n = 6) compared with that in peripheral blood mononuclear cells from asymptomatic carriers (AC, n = 5). These cells were cultured without any stimuli for 24, 48 and 72 h. ND = not detected. (**B**) Concentrations of IFN-γ (*left*) and IL-17A (*right*) in culture supernatants of cultured CD4$^+$ T cells for 72 h from patients with HAM/TSP compared with the concentrations in those from asymptomatic carriers. Patients with HAM/TSP: n = 6, asymptomatic carrier: n = 5. ND = not detected. Statistical analyses were performed using the Mann–Whitney U-test. (**C**) Concentration of CXCL10 produced by U251, a human astrocytoma cell line, co-cultured with CD4$^+$ T cells from patients with HAM/TSP (n = 5). ND = not detected. (**D**) Concentration of CXCL10 produced by U251 stimulated by the supernatant of cultured CD4$^+$ T cells of patients with HAM/TSP (n = 5) in the presence of neutralizing antibodies against IFN-γ and TNF-α, and isotype control antibodies for each. NS = not significant. **$P < 0.01$. Error bars represent the mean ± SD.

significant). Next, we investigated whether or not this decreased migration would also be reflected in the absolute number of HTLV-1-infected cells among migrated cells. Chemotaxis assays revealed that the addition of human CXCL10 (0.25 μg/ml) increased the absolute number of HTLV-1-infected cells by ~2.1-fold (Fig. 5B) compared with isotype control monoclonal antibodies, and that this increase was largely inhibited by anti-CXCL10 neutralizing antibodies (Fig. 5B; 101.1% inhibition, $P < 0.01$) but only slightly by anti-CXCR3 antibodies (Fig. 5B; 65.7% inhibition, $P > 0.05$: not significant). Finally, we evaluated the degree to which the migrated cells were proliferating spontaneously, where spontaneous proliferation is defined as proliferation in the absence of exogenous antigens or stimulants (Itoyama *et al.*, 1988; Ijichi *et al.*, 1989). This is important because the level of spontaneous proliferation of peripheral blood mononuclear cells in patients with HAM/TSP is believed to reflect the cell proliferation that occurs in the CNS (Itoyama *et al.*, 1988; Ijichi *et al.*, 1989). Significantly less ^{3}H-thymidine uptake, an assay for cell proliferation, was detected in the lower chemotaxis assay chamber following administration of anti-CXCL10 antibody than isotype control antibodies (Fig. 5C; 33.8% inhibition, $P < 0.05$).

Discussion

Previous studies of HAM/TSP pathogenesis have revealed that chronic inflammation occurs in the spinal cords of patients with HAM/TSP (Saito and Bangham, 2012; Yamano and Sato, 2012);

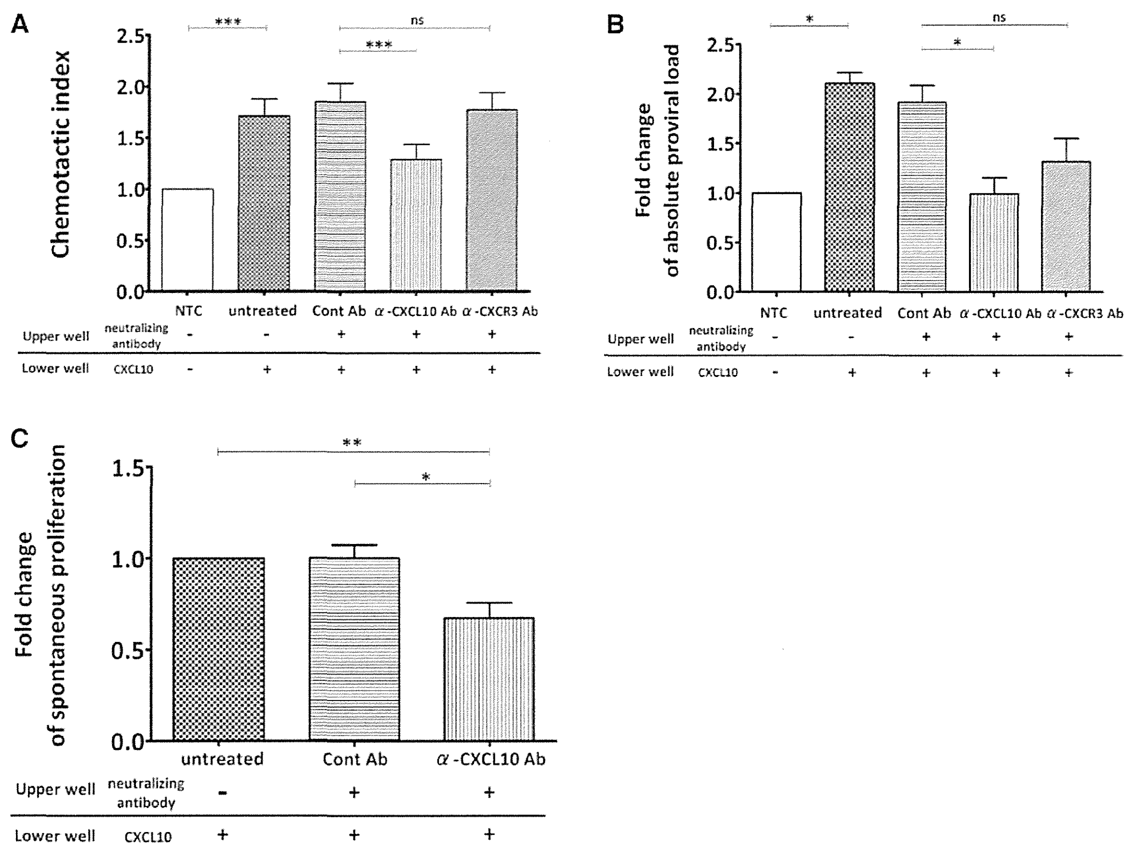

Figure 5 Chemotaxis of peripheral blood mononuclear cells due to CXCL10 and inhibition of chemotaxis by anti-CXCL10 neutralizing antibody in cells from patients with HAM/TSP. (**A**) The migration-inducing effect of CXCL10 and the inhibitory effect of neutralizing antibody against CXCL10 versus its receptor, CXCR3. Peripheral blood mononuclear cells from patients with HAM/TSP (n = 21) migrated into the lower well in response to CXCL10, and treatment with anti-CXCL10 antibody significantly reduced the migration of peripheral blood mononuclear cells, as compared to anti-CXCR3 antibody and control antibody. (**B**) The inhibition of cell migration led to an overall decrease in migrated cells including HTLV-1-infected cells, effectively decreasing the absolute proviral load. Peripheral blood mononuclear cells used were collected from patients with HAM/TSP; $n = 4$. (**C**) The inhibition of cell migration led to an overall decrease in migrated cells which also means less spontaneous proliferation. Peripheral blood mononuclear cells used were collected from patients with HAM/TSP; $n = 7$. Error bars represent the mean ± SD. Statistical analyses were performed using the Friedman test followed by the Dunn test for multiple comparison. NS = not significant. $*P < 0.05$, $**P < 0.01$, $***P < 0.001$. NTC = negative control; Cont Ab = isotype control monoclonal antibody; α-CXCL10 Ab = anti-CXCL10 monoclonal antibody; α-CXCR3 Ab = anti-CXCR3 monoclonal antibody.

however, the precise mechanisms by which these inflammatory lesions are formed and maintained remain unclear. We hypothesized that a positive feedback loop driven by chemokines may be responsible for the chronic inflammation associated with HAM/TSP. We identified CXCL10 as the principal chemokine responsible for inducing this chronic inflammation. We found for the first time astrocytes to be the main producers of CXCL10. Our data suggest that these astrocytes are stimulated to produce CXCL10 initially by IFN-γ released by infected T cells, where the infection appears to have produced changes in the cells that promote spontaneous IFN-γ production. In short, we inferred that spinal cord lesions found in patients with HAM/TSP arise when IFN-γ produced by HTLV-1-infected T cells induces astrocytes to secrete CXCL10, which attracts $CXCR3^+$ T cells, including more T cells infected with HTLV-1, thereby continuing the cycle. Furthermore, we demonstrated that an interruption of this pathway represents a promising strategy for treating HAM/TSP.

First, we identified the key chemokine involved in inducing the migration of cells to sites of inflammation. We compared the CSF and serum levels of several chemokines and demonstrated for the first time that CXCL10 is the only chemokine of those studied that is present at a significantly higher concentration in the CSF than in the sera of patients with HAM/TSP. Although previous reports indicate that CCL5 and CXCL9 levels are also elevated in the CSF of patients with HAM/TSP (Teixeira *et al.*, 2004; Tanaka *et al.*, 2008), we showed that these two chemokines exhibit a concentration gradient in the opposite direction (Fig. 1B). We previously measured the levels of other chemokines such as CCL3, CCL4, CXCL11, CCL17, CCL20 and CCL22 in the CSF and found that the levels of these chemokines are negligible in patients with HAM/TSP (Sato, in press). Importantly, we also previously demonstrated that CSF CXCL10 levels are correlated with the rate of disease progression (Sato, in press). These findings suggest that CXCL10 is crucial for the development of chronic inflammation in patients with HAM/TSP.

In the present study, we found a positive correlation between CSF CXCL10 levels and CSF cell counts (Fig. 1A), a high percentage of CXCR3-positive cells in the CSF (Fig. 2A and B; 92.4 ± 7.0%), and perivascular accumulation of CXCR3$^+$ cells in spinal cord lesions of patients with HAM/TSP (Fig. 2C). These results strongly indicate that a high concentration of CXCL10 in the spinal cord attracts CXCR3$^+$ cells that include proinflammatory cells (Qin *et al.*, 1998; Sallusto *et al.*, 1998; Thomas *et al.*, 2003). Intriguingly, the percentage of CXCR3$^+$ cells among peripheral blood mononuclear cells from patients with HAM/TSP was significantly lower than that observed in asymptomatic carriers and healthy donors, but not patients with adult T cell leukaemia (Supplementary Fig. 3). CXCR3$^+$ peripheral blood mononuclear cells are relatively few in patients with adult T cell leukaemia, perhaps because of an increase in CCR4$^+$CXCR3$^-$ tumour cells in the peripheral blood (Ishida *et al.*, 2003). Although the precise mechanism by which peripheral CXCR3$^+$ cells in patients with HAM/TSP become diminished remains unclear, we believe that many of these cells migrate into the CNS and contribute to the formation of spinal cord lesions. Other possible mechanisms include migration to lymphoid organs such as lymph nodes or the spleen. Because lymph nodes are important organs for CXCL10–CXCR3 interactions in patients suffering from various diseases (Groom *et al.*, 2012; Sung *et al.*, 2012), future studies analysing the lymph nodes of patients with HAM/TSP may provide a more complete understanding of HAM/TSP pathogenesis.

The discovery that CXCL10–CXCR3 interactions represent an important pathway for recruiting cells to the CNS in patients with HAM/TSP prompted us to search the spinal cord lesions of patients with HAM/TSP and identify the CXCL10-producing cells. Firstly, we confirmed that CXCL10-producing cells are more numerous in the spinal cords of patients with HAM/TSP than control individuals (Fig. 3A). We also compared high and low inflammatory regions within a single patient with HAM/TSP and found more CXCL10-producing cells in the more inflamed region (Supplementary Fig. 4), although the limitation of sampling from only a single individual prevents us from extrapolating too freely on the significance of this result. Although CXCL10 is secreted by several cell types such as monocytes, endothelial cells, fibroblasts and astrocytes in response to IFN-γ (Luster and Ravetch, 1987; Lee *et al.*, 2009), our study demonstrated that astrocytes are the major CXCL10-producing cells in thoracic spinal cord lesions in patients with HAM/TSP (Fig. 3). Notably, the astrocytes examined in this study were star-shaped with radiating cytoplasmic processes, indicating high cytological activity (Fig. 3B and C). In the CNS, CXCL10 is mainly produced by astrocytes; however, CXCL9 is primarily a product of microglial cells (Muller *et al.*, 2010). Therefore, the finding that CXCL10 production is substantially higher than CXCL9 production in the CSF (Fig. 1) suggests that astrocytes are very active in HAM/TSP. This finding supports a previous finding that gliosis is one of the main pathological features of HAM/TSP (Iwasaki, 1990; Izumo *et al.*, 1992).

Next, we investigated the mechanism by which astrocytes produce CXCL10 in patients with HAM/TSP. CXCL10 is generally not detectable in most non-lymphoid tissues under physiological conditions; however, its synthesis is easily induced by cytokines, particularly IFN-γ. Therefore, it was important to determine the source of IFN-γ that stimulates astrocytes to produce CXCL10 in patients with HAM/TSP. Interestingly, we have shown that CD4$^+$ T cells from patients with HAM/TSP spontaneously produce IFN-γ and induce CXCL10 production by U251 human astrocytoma cells via IFN-γ (Fig. 4), whereas CD4$^+$ T cells from healthy donors do not induce CXCL10 production (data not shown). These results support the hypothesis that there are interactions between HTLV-1-infected CD4$^+$ T cells and astrocytes in patients with HAM/TSP *in vivo* that may possibly initiate the first wave of CXCL10 production. Moreover, this CXCL10 production may further induce the trafficking of peripheral CXCR3$^+$ T cells. Importantly, we demonstrated that a number of peripheral CXCR3$^+$ T cells are infected with HTLV-1 (Fig. 2E), indicating that migration of peripheral CXCR3$^+$ T cells into the CNS can induce further secretion of IFN-γ that continues the vicious cycle. In fact, HTLV-1-infected CD4$^+$ T cells and IFN-γ-producing T cells have been detected in HAM/TSP spinal cord lesions (Umehara *et al.*, 1994; Moritoyo *et al.*, 1996; Matsuoka *et al.*, 1998). Notably, more than half of the CXCR3$^+$ T cells in the CSF of patients with HAM/TSP are CD8$^+$ T cells (Fig. 2D). It has been shown that CD8$^+$ cytotoxic T lymphocytes (CTLs), particularly HTLV-1-specific CTLs, have a high potential for secreting IFN-γ (Kubota *et al.*, 2000; Hanon *et al.*, 2001) and are abnormally elevated in the CSF and spinal cord lesions (Nagai *et al.*, 2001*a*, *b*; Matsuura *et al.*, 2010). Therefore, CXCL10 production by astrocytes may further boost the trafficking of CXCR3$^+$-infected CD4$^+$ T cells as well as CXCR3$^+$CD8$^+$ CTLs that secrete IFN-γ, leading to a positive feedback-driven chronic inflammatory loop.

The results of the present study and other studies show that the pathology of HAM/TSP is unique among immune disorders. Unlike other inflammatory disorders such as multiple sclerosis or rheumatoid arthritis that exhibit Th17 as well as Th1 involvement (Matusevicius *et al.*, 1999; Kirkham *et al.*, 2006), HAM/TSP pathogenesis appears to be dominated by the Th1 axis, particularly CXCL10–CXCR3 interactions. Our research indicates that the characteristics of HTLV-1-infected T cells may be responsible for the emphasis on the Th1 axis in HAM/TSP pathogenesis. We have reported that cultured CD4$^+$ T cells from patients with HAM/TSP clearly exhibit detectable production of IFN-γ (a Th1 cytokine) but not IL-17 (a Th17 cytokine) (Fig. 4B), and we previously demonstrated that HTLV-1-infected T cells in patients with HAM/TSP exhibit elevated IFN-γ and reduced IL-17 production (Yamano *et al.*, 2009). Furthermore, HAM/TSP peripheral blood contained more CXCL10 (Supplementary Fig. 1B) and fewer CXCR3$^+$ cells (Supplementary Fig. 3B) than asymptomatic carrier blood, suggesting that a greater number of CXCR3$^+$ cells had migrated out of the periphery due at least in part to chemotaxis induced by elevated CXCL10 production in the CNS. As the proviral loads of all the samples used in the above experiment were roughly identically high, it can be assumed that these characteristics are indeed features of HAM/TSP pathogenesis as opposed to simple consequences of having a high proviral load.

We suspect that a genetic predisposition for higher IFN-γ or CXCL10 production in response to HTLV-1 may exist. Recently, systems biology approaches were used to show that a subset of IFN-stimulated genes, including the gene encoding CXCL10, is overexpressed in peripheral blood mononuclear cells of patients with HAM/TSP compared with asymptomatic carriers

(Tattermusch *et al.*, 2012). It will be important to test for an association between genetic polymorphisms in interferon-associated genes and the presence of HAM/TSP in future studies. The existence of this genetic predisposition would strengthen the argument for Th1-dominance and explain why some infected individuals develop HAM/TSP, whereas others remain life-long asymptomatic carriers. Because it is well-known that interferons and products of interferon-stimulated genes mediate antiviral responses (Randall and Goodbourn, 2008), IFN-γ and CXCL10 production in HTLV-1-infected patients (Supplementary Fig. 1) may be considered a normal immune response. However, once the production levels surpass threshold and a CXCL10–CXCR3 amplification loop develops, it may begin to cause tissue damage. Possible reasons for CXCL10 overproduction in HAM/TSP include the presence of a high number of HTLV-1-infected T cells (Nagai *et al.*, 1998; Yamano *et al.*, 2002) and a genetic predisposition for higher IFN-γ and/or CXCL10 production in response to HTLV-1.

The ideal therapeutic strategy for treating HAM/TSP would be eradication of HTLV-1-infected cells, but this has yet to be proven possible. Another promising approach would be a receptor blockade using anti-CXCR3 neutralizing antibody, which has been reported to be effective at blocking CXCR3 activity (Van den Steen *et al.*, 2008). Although we were unable to validate this effect using our commercially available antibody, this certainly does not rule out a receptor blockade as a therapeutic candidate. Our relative success at disrupting inflammatory cell migration using anti-CXCL10 neutralizing antibodies (Fig. 5) suggests that targeting CXCL10 to interrupt the positive feedback loop may be the more promising new strategy for effectively treating HAM/TSP. A noteworthy potential advantage of anti-CXCL10 over anti-CXCR3 is that it may yield less severe side effects as only interactions with CXCL10 rather than all CXCR3 agonists would be blocked.

In conclusion, our data revealed novel insights into the pathogenic processes of HAM/TSP. Our results suggest that CXCL10 plays a pivotal role in the development of chronic inflammatory lesions where HTLV-1-infected T cells produce IFN-γ, which induces astrocytes to secrete CXCL10. This further boosts the trafficking of $CXCR3^{+}$-infected T cells that secrete IFN-γ, leading to a virus-induced CXCL10–CXCR3 inflammatory loop. Thus, HAM/TSP represents a pathological consequence of interactions that occur between the immune system and CNS. Understanding these complex interactions should provide new insights into the functional regulation of both systems and help uncover new therapeutic targets.

Acknowledgements

The authors thank K. Takahashi, Y. Kunitomo, Y. Sato, Y. Suzuki, M. Koike, and Y. Hasegawa for technical assistance.

Funding

This work was partly supported by project "Research on Measures for Intractable Disease," a matching fund subsidy from the Ministry of Health Labour and Welfare, a Grant-in-Aid for Scientific Research from the Ministry of Education, Culture, Sports, Science and Technology, and the MEXT-Supported Program for the Strategic Research Foundation at Private Universities, 2008–2012.

Supplementary material

Supplementary material is available at *Brain* online.

References

Furuya T, Nakamura T, Shirabe S, Nishiura Y, Tsujino A, Goto H, et al. Heightened transmigrating activity of CD4-positive T cells through reconstituted basement membrane in patients with human T-lymphotropic virus type I-associated myelopathy. Proc Assoc Am Physicians 1997; 109: 228–36.

Gessain A, Barin F, Vernant JC, Gout O, Maurs L, Calender A, et al. Antibodies to human T-lymphotropic virus type-I in patients with tropical spastic paraparesis. Lancet 1985; 2: 407–10.

Goon PK, Hanon E, Igakura T, Tanaka Y, Weber JN, Taylor GP, et al. High frequencies of Th1-type CD4(+) T cells specific to HTLV-1 env and tax proteins in patients with HTLV-1-associated myelopathy/tropical spastic paraparesis. Blood 2002; 99: 3335–41.

Groom JR, Richmond J, Murooka TT, Sorensen EW, Sung JH, Bankert K, et al. CXCR3 chemokine receptor-ligand interactions in the lymph node optimize CD4(+) T helper 1 cell differentiation. Immunity 2012; 37: 1091–103.

Hanon E, Goon P, Taylor GP, Hasegawa H, Tanaka Y, Weber JN, et al. High production of interferon gamma but not interleukin-2 by human T-lymphotropic virus type I-infected peripheral blood mononuclear cells. Blood 2001; 98: 721–6.

Hinuma Y, Nagata K, Hanaoka M, Nakai M, Matsumoto T, Kinoshita KI, et al. Adult T-cell leukemia: antigen in an ATL cell line and detection of antibodies to the antigen in human sera. Proc Natl Acad Sci USA 1981; 78: 6476–80.

Ijichi S, Eiraku N, Osame M, Izumo S, Kubota R, Maruyama I, et al. In vitro modulation of lymphocyte proliferation by prednisolone and interferon-alpha in patients with HTLV-I-associated myelopathy (HAM). J Neuroimmunol 1989; 23: 175–8.

Ishida T, Utsunomiya A, Iida S, Inagaki H, Takatsuka Y, Kusumoto S, et al. Clinical significance of CCR4 expression in adult T-cell leukemia/lymphoma: its close association with skin involvement and unfavorable outcome. Clin Cancer Res 2003; 9: 3625–34.

Itoyama Y, Minato S, Kira J, Goto I, Sato H, Okochi K, et al. Spontaneous proliferation of peripheral blood lymphocytes increased in patients with HTLV-I-associated myelopathy. Neurology 1988; 38: 1302–7.

Iwasaki Y. Pathology of chronic myelopathy associated with HTLV-I infection (HAM/TSP). J Neurol Sci 1990; 96: 103–23.

Izumo S, Ijichi T, Higuchi I, Tashiro A, Takahashi K, Osame M. Neuropathology of HTLV-I-associated myelopathy—a report of two autopsy cases. Acta Paediatr Jpn 1992; 34: 358–64.

Jacobson S, Shida H, McFarlin DE, Fauci AS, Koenig S. Circulating CD8(plus) cytotoxic T lymphocytes specific for HTLV-I pX in patients with HTLV-I associated neurological disease. Nature 1990; 348: 245–8.

Jeffery KJ, Usuku K, Hall SE, Matsumoto W, Taylor GP, Procter J, et al. HLA alleles determine human T-lymphotropic virus-I (HTLV-I) proviral load and the risk of HTLV-I-associated myelopathy. Proc Natl Acad Sci USA 1999; 96: 3848–53.

Kirkham BW, Lassere MN, Edmonds JP, Juhasz KM, Bird PA, Lee CS, et al. Synovial membrane cytokine expression is predictive of joint damage progression in rheumatoid arthritis: a two-year prospective study (the DAMAGE study cohort). Arthritis Rheum 2006; 54: 1122–31.

Kubota R, Kawanishi T, Matsubara H, Manns A, Jacobson S. HTLV-I specific IFN-gamma+ CD8+ lymphocytes correlate with the proviral load in peripheral blood of infected individuals. J Neuroimmunol 2000; 102: 208–15.

Downloaded from http://brain.oxfordjournals.org/ at St. Marianna University School of Medicine on July 25, 2013

Lee EY, Lee ZH, Song YW. CXCL10 and autoimmune diseases. Autoimmun Rev 2009; 8: 379–83.
Libby P. Inflammation in atherosclerosis. Nature 2002; 420: 868–74.
Luster AD. Chemokines—chemotactic cytokines that mediate inflammation. N Engl J Med 1998; 338: 436–45.
Luster AD, Ravetch JV. Biochemical characterization of a gamma interferon-inducible cytokine (IP-10). J Exp Med 1987; 166: 1084–97.
Mantovani A, Allavena P, Sica A, Balkwill F. Cancer-related inflammation. Nature 2008; 454: 436–44.
Matsuoka E, Takenouchi N, Hashimoto K, Kashio N, Moritoyo T, Higuchi I, et al. Perivascular T cells are infected with HTLV-I in the spinal cord lesions with HTLV-I-associated myelopathy/tropical spastic paraparesis: double staining of immunohistochemistry and polymerase chain reaction in situ hybridization. Acta Neuropathol 1998; 96: 340–6.
Matsuura E, Yamano Y, Jacobson S. Neuroimmunity of HTLV-I infection. J Neuroimmune Pharmacol 2010; 5: 310–25.
Matusevicius D, Kivisakk P, He B, Kostulas N, Ozenci V, Fredrikson S, et al. Interleukin-17 mRNA expression in blood and CSF mononuclear cells is augmented in multiple sclerosis. Mult Scler 1999; 5: 101–4.
Medzhitov R. Inflammation 2010: new adventures of an old flame. Cell 2010; 140: 771–6.
Medzhitov R. Origin and physiological roles of inflammation. Nature 2008; 454: 428–35.
Moritoyo H, Arimura K, Arimura Y, Tokimura Y, Rosales R, Osame M. Study of lower limb somatosensory evoked potentials in 96 cases of HTLV-I-associated myelopathy/tropical spastic paraparesis. J Neurol Sci 1996; 138: 78–81.
Muller M, Carter S, Hofer MJ, Campbell IL. Review: the chemokine receptor CXCR3 and its ligands CXCL9, CXCL10 and CXCL11 in neuroimmunity—a tale of conflict and conundrum. Neuropathol Appl Neurobiol 2010; 36: 368–87.
Nagai M, Yamano Y, Brennan MB, Mora CA, Jacobson S. Increased HTLV-I proviral load and preferential expansion of HTLV-I tax-specific CD8+ T cells in cerebrospinal fluid from patients with HAM/TSP. Ann Neurol 2001a; 50: 807–12.
Nagai M, Brennan MB, Sakai JA, Mora CA, Jacobson S. CD8(+) T cells are an *in vivo* reservoir for human T-cell lymphotropic virus type I. Blood 2001b; 98: 1858–61.
Nagai M, Usuku K, Matsumoto W, Kodama D, Takenouchi N, Moritoyo T, et al. Analysis of HTLV-I proviral load in 202 HAM/TSP patients and 243 asymptomatic HTLV-I carriers: high proviral load strongly predisposes to HAM/TSP. J Neurovirol 1998; 4: 586–93.
Narikawa K, Fujihara K, Misu T, Feng J, Fujimori J, Nakashima I, et al. CSF-chemokines in HTLV-I-associated myelopathy: CXCL10 up-regulation and therapeutic effect of interferon-alpha. J Neuroimmunol 2005; 159: 177–82.
Nie CQ, Bernard NJ, Norman MU, Amante FH, Lundie RJ, Crabb BS, et al. IP-10-mediated T cell homing promotes cerebral inflammation over splenic immunity to malaria infection. PLoS Pathog 2009; 5: e1000369.
Osame M. Review of WHO kagoshima meeting and diagnostic guidelines for HAM/TSP. In: Blattner WA, editor. Human retrovirology: HTLV. New York: Raven Press, 1990. p. 191–7.
Osame M, Usuku K, Izumo S, Ijichi N, Amitani H, Igata A, et al. HTLV-I associated myelopathy, a new clinical entity. Lancet 1986; 1: 1031–2.
Proost P, Vynckier AK, Mahieu F, Put W, Grillet B, Struyf S, et al. Microbial toll-like receptor ligands differentially regulate CXCL10/IP-10 expression in fibroblasts and mononuclear leukocytes in synergy with IFN-gamma and provide a mechanism for enhanced synovial chemokine levels in septic arthritis. Eur J Immunol 2003; 33: 3146–53.
Proost P, Schutyser E, Menten P, Struyf S, Wuyts A, Opdenakker G, et al. Amino-terminal truncation of CXCR3 agonists impairs receptor signaling and lymphocyte chemotaxis, while preserving antiangiogenic properties. Blood 2001; 98: 3554–61.
Qin S, Rottman JB, Myers P, Kassam N, Weinblatt M, Loetscher M, et al. The chemokine receptors CXCR3 and CCR5 mark subsets of T cells associated with certain inflammatory reactions. J Clin Invest 1998; 101: 746–54.
Randall RE, Goodbourn S. Interferons and viruses: an interplay between induction, signalling, antiviral responses and virus countermeasures. J Gen Virol 2008; 89: 1–47.
Richardson JH, Edwards AJ, Cruickshank JK, Rudge P, Dalgleish AG. *In vivo* cellular tropism of human T-cell leukemia virus type 1. J Virol 1990; 64: 5682–7.
Saito M, Bangham CR. Immunopathogenesis of human T-cell leukemia virus type-1-associated myelopathy/tropical spastic paraparesis: recent perspectives. Leuk Res Treatment 2012; 2012: 259045.
Sallusto F, Lenig D, Mackay CR, Lanzavecchia A. Flexible programs of chemokine receptor expression on human polarized T helper 1 and 2 lymphocytes. J Exp Med 1998; 187: 875–83.
Shimoyama M. Diagnostic criteria and classification of clinical subtypes of adult T-cell leukaemia-lymphoma. A report from the lymphoma study group (1984–87). Br J Haematol 1991; 79: 428–37.
Sung JH, Zhang H, Moseman EA, Alvarez D, Iannacone M, Henrickson SE, et al. Chemokine guidance of central memory T cells is critical for antiviral recall responses in lymph nodes. Cell 2012; 150: 1249–63.
Tanaka M, Matsushita T, Tateishi T, Ochi H, Kawano Y, Mei FJ, et al. Distinct CSF cytokine/chemokine profiles in atopic myelitis and other causes of myelitis. Neurology 2008; 71: 974–81.
Tattermusch S, Skinner JA, Chaussabel D, Banchereau J, Berry MP, McNab FW, et al. Systems biology approaches reveal a specific interferon-inducible signature in HTLV-1 associated myelopathy. PLoS Pathog 2012; 8: e1002480.
Teixeira AL Jr, Cardoso F, Souza AL, Teixeira MM. Increased serum concentrations of monokine induced by interferon-gamma/CXCL9 and interferon-gamma-inducible protein 10/CXCL-10 in sydenham's chorea patients. J Neuroimmunol 2004; 150: 157–62.
Thomas SY, Hou R, Boyson JE, Means TK, Hess C, Olson DP, et al. CD1d-restricted NKT cells express a chemokine receptor profile indicative of Th1-type inflammatory homing cells. J Immunol 2003; 171: 2571–80.
Umehara F, Izumo S, Ronquillo AT, Matsumuro K, Sato E, Osame M. Cytokine expression in the spinal cord lesions in HTLV-I-associated myelopathy. J Neuropathol Exp Neurol 1994; 53: 72–7.
Van den Steen PE, Deroost K, Van Aelst I, Geurts N, Martens E, Struyf S, et al. CXCR3 determines strain susceptibility to murine cerebral malaria by mediating T lymphocyte migration toward IFN-gamma-induced chemokines. Eur J Immunol 2008; 38: 1082–95.
Waldmann TA. The biology of interleukin-2 and interleukin-15: implications for cancer therapy and vaccine design. Nat Rev Immunol 2006; 6: 595–601.
Yamano Y, Sato T. Clinical pathophysiology of human T-lymphotropic virus-type 1-associated myelopathy/tropical spastic paraparesis. Front Microbiol 2012; 3: 389.
Yamano Y, Takenouchi N, Li HC, Tomaru U, Yao K, Grant CW, et al. Virus-induced dysfunction of CD4+CD25+ T cells in patients with HTLV-I-associated neuroimmunological disease. J Clin Invest 2005; 115: 1361–8.
Yamano Y, Nagai M, Brennan M, Mora CA, Soldan SS, Tomaru U, et al. Correlation of human T-cell lymphotropic virus type 1 (HTLV-1) mRNA with proviral DNA load, virus-specific CD8(+) T cells, and disease severity in HTLV-1-associated myelopathy (HAM/TSP). Blood 2002; 99: 88–94.
Yamano Y, Araya N, Sato T, Utsunomiya A, Azakami K, Hasegawa D, et al. Abnormally high levels of virus-infected IFN-gamma+ CCR4+ CD4+ CD25+ T cells in a retrovirus-associated neuroinflammatory disorder. PLoS One 2009; 4: e6517.
Yasuda N, Lai PK, Ip SH, Kung PC, Hinuma Y, Matsuoka M, et al. Soluble interleukin 2 receptors in sera of japanese patients with adult T cell leukemia mark activity of disease. Blood 1988; 71: 1021–6.

From bloodjournal.hematologylibrary.org at ST MARIANNA SCHOOL on May 29, 2013. For personal use only.

Regular Article

LYMPHOID NEOPLASIA

Preapoptotic protease calpain-2 is frequently suppressed in adult T-cell leukemia

Makoto Ishihara,[1] Natsumi Araya,[2] Tomoo Sato,[2] Ayako Tatsuguchi,[1] Naomi Saichi,[1] Atae Utsunomiya,[3] Yusuke Nakamura,[4] Hidewaki Nakagawa,[1] Yoshihisa Yamano,[2] and Koji Ueda[1]

[1]Laboratory for Biomarker Development, Center of Genomic Medicine, RIKEN, Tokyo, Japan; [2]Department of Molecular Medical Science, Institute of Medical Science, St. Marianna University School of Medicine, Kawasaki, Japan; [3]Department of Hematology, Imamura Bun-in Hospital, Kagoshima, Japan; and [4]Section of Hematology/Oncology, Department of Medicine Faculty, The University of Chicago, Chicago, IL

Key Points

- Proteome-wide analysis of HTLV-1–infected T cells identified 17 biomarker proteins for the diagnosis of ATL or HAM/TSP patients.

Adult T-cell leukemia (ATL) is one of the most aggressive hematologic malignancies caused by human T-lymphotropic virus type 1 (HTLV-1) infection. The prognosis of ATL is extremely poor; however, effective strategies for diagnosis and treatment have not been established. To identify novel therapeutic targets and diagnostic markers for ATL, we employed focused proteomic profiling of the CD4$^+$CD25$^+$CCR4$^+$ T-cell subpopulation in which HTLV-1–infected cells were enriched. Comprehensive quantification of 14 064 peptides and subsequent 2-step statistical analysis using 29 cases (6 uninfected controls, 5 asymptomatic carriers, 9 HTLV-1–associated myelopathy/tropical spastic paraparesis patients, 9 ATL patients) identified 91 peptide determinants that statistically classified 4 clinical groups with an accuracy rate of 92.2% by cross-validation test. Among the identified 17 classifier proteins, α-II spectrin was drastically accumulated in infected T cells derived from ATL patients, whereas its digestive protease calpain-2 (CAN2) was significantly downregulated. Further cell cycle analysis and cell growth assay revealed that rescue of CAN2 activity by overexpressing constitutively active CAN2 (Δ_{19}CAN2) could induce remarkable cell death on ATL cells accompanied by reduction of α-II spectrin. These results support that proteomic profiling of HTLV-1–infected T cells could provide potential diagnostic biomarkers and an attractive resource of therapeutic targets for ATL. (*Blood.* 2013;121(21):4340-4347)

Introduction

Human T-lymphotropic virus type 1 (HTLV-1) is a human retrovirus that is the pathogenic agent of HTLV-1–associated diseases, such as adult T-cell leukemia (ATL) and HTLV-1–associated myelopathy/tropical spastic paraparesis (HAM/TSP). Recent epidemiological studies revealed that HTLV-1 is endemic mainly in Japan, the Caribbean basin, Iran, Africa, South America, and the Melanesian islands.[1] Other estimates have shown that 20 million to 30 million people worldwide are infected with HTLV-1.[2] The infection is followed by a prolonged asymptomatic phase of 20 to 30 years, and 2% to 5% of the infected individuals develop ATL during their lifetime.[3] ATL is one of the most aggressive hematologic malignancies characterized by increased numbers of lymphocytes with multilobulated nuclei, so-called flower cells, in blood circulation. The prognosis is severe with the median overall survival period and 5-year survival rate of ATL patients of 7 months and 20%, respectively.[4] Recently, humanized anti-CCR4 (KW-0761) therapeutic antibody achieved a great improvement in ATL treatment in a phase 3 study. However, the disease control rate was restricted to 50%, and long-term prognosis has yet to be known.[5] For future improvements in the management of ATL, novel biomarkers for early diagnosis are urgently needed for early therapeutic intervention.

To date, comprehensive genomic or proteomic studies using CD4$^+$ T cells have been performed for this purpose,[6-9] but reproducibility and reliability of quantification results in the discovery phase were uncertain due to the diverse individual variety of HTLV-1–infected cell contents in CD4$^+$ T cells. To overcome the etiologic variety of samples, we focused on the CD4$^+$CD25$^+$CCR4$^+$ T-cell subpopulation since Yamano et al[10] recently revealed that HTLV-1 preferentially infected CD4$^+$CD25$^+$CCR4$^+$ T cells in both ATL and HAM/TSP patients. By targeting CD4$^+$CD25$^+$CCR4$^+$ T cells, we here provide the first quantitative proteome map illustrating molecular disorders in pathogenic human T cells directly associated with the onset or progression of ATL. The comprehensive and comparative interpretation of total proteome in infected cells, especially between asymptomatic HTLV-1 carriers and ATL patients, could immediately lead to specific candidates for biomarkers and drugs.

Another challenge to emphasize in this study is our recently established proteomic profiling technologies. It is indisputable that the greater the number of clinical samples analyzed, the more confidently statistical analysis can be undertaken in order to identify diagnostic markers and druggable targets. Despite this fact, previous proteomics reports could not provide high-throughput quantitative methodologies that were sufficient for dealing with even more than 10 clinical samples, excepting a study utilizing a surface enhanced laser desorption/ionization time of flight mass spectrometer. Although the surface enhanced laser desorption/ionization time of flight method drastically improved the performance in both quantification and throughput, allowing relative quantification

Submitted August 1, 2012; accepted March 25, 2013. Prepublished online as *Blood* First Edition paper, March 28, 2013; DOI 10.1182/blood-2012-08-446922.

The online version of this article contains a data supplement.

The publication costs of this article were defrayed in part by page charge payment. Therefore, and solely to indicate this fact, this article is hereby marked "advertisement" in accordance with 18 USC section 1734.

© 2013 by The American Society of Hematology

From bloodjournal.hematologylibrary.org at ST MARIANNA SCHOOL on May 29, 2013. For personal use only.

analysis for 96 samples in several hours, at most only 250 unidentified protein peaks were detectable. In the present study, we integrated the proteomics server for the huge data set "Expressionist" (Genedata A.G., Basel, Switzerland) with high-end mass spectrometers to maximize the quality and quantity of protein catalogs transferred from mass spectrometers. We first describe the discovery phase providing a panel of novel diagnostic molecules from quantification of 14 064 peptides and identification of 4763 proteins. As the functional validation phase, we further examined the physiological potential of an identified diagnostic marker candidate, calpain-2 (CAN2), particularly concerning the association of its activity with survival or progression of ATL cells.

Materials and methods

PBMCs and cell lines

Peripheral blood mononuclear cells (PBMCs) from 6 normal donors, 5 asymptomatic carriers, and 9 HAM/TSP patients used in the screening analysis were collected in the St. Marianna University School of Medicine. Those from 9 ATL patients were collected in the Imamura Bun-in Hospital. PBMCs from 4 ATL patients used for the validation experiments were provided by the Joint Study on Predisposing Factors of ATL Development. The others from 4 HAM/TSP patients were collected in the St. Marianna University School of Medicine. The use of these human specimens in this study was approved by individual institutional ethical committees: the Ethical Committee of Yokohama Institute, RIKEN (approval code Yokohama H22-3); the Ethical Committee of St. Marianna University School of Medicine; the Institutional Review Board of Imamura Bun-in Hospital; and the Ethical Committee of the University of Tokyo (approval code 10-50). This study was conducted in accordance with the Declaration of Helsinki.

SO-4, KOB, and KK1 cells were kindly provided by Dr Yasuaki Yamada, cultured in RPMI 1640 supplemented with 10% fetal bovine serum (Cell Culture Bioscience, Tokyo, Japan), 100 kU/L interleukin 2 (Cell Science & Technology Institute Inc., Tokyo, Japan), and 1 × antibiotic-antimycotic solution (Sigma-Aldrich, MO). Jurkat, SUP-T1, CCRF-CEM, and MOLT-3 cells were cultured in RPMI 1640 supplemented with 10% fetal bovine serum and 1 × antibiotic-antimycotic solution. All cell lines were grown at 37°C in 5% CO_2. $CD3^+CD4^+CD25^+CCR4^+$ T cells were isolated with anti-CD3-FITC (eBioscience, San Diego, CA), anti-CCR4-PE (Becton Dickinson, CA), anti-CD4-Cy7 (eBioscience), and anti-CD25-APC (eBioscience) on a Cell Sorter JSAN (Bay Bioscience, Hyogo, Japan).

Sample preparation for mass spectrometric analysis

The $CD4^+CD25^+CCR4^+$ T cells were washed with phosphate-buffered saline 3 times and lysed in denaturation buffer (8 M urea in 50 mM ammonium bicarbonate). After sonication, reduction with 5 mM tris(2-carboxyethyl) phosphine (Sigma-Aldrich) at 37°C for 30 minutes, and alkylation with 25 mM iodacetamide (Sigma-Aldrich) at room temperature for 45 minutes, lysates were digested with Trypsin GOLD (Promega, WI) with protein/enzyme ratio of 25:1 at 37°C for 12 hours. The digested peptides were desalted with Oasis HLB μElution plate (Waters, MA). The collected samples were dried up with a Vacuum Spin Drier (TAITEC Co. Ltd., Saitama, Japan) and subjected to mass spectrometric analyses.

Liquid chromatography tandem mass spectrometry (LC/MS/MS)

The digested peptides were separated on a 0.1 × 200 mm homemade C_{18} column using a 2-step linear gradient, 2% to 35% acetonitrile for 95 minutes and 35% to 95% acetonitrile for 15 minutes in 0.1% formic acid with a flow rate of 200 nL/min. The eluting peptides were analyzed with a QSTAR-Elite mass spectrometer (AB Sciex, CA) in the smart information-dependent acquisition mode of Analyst QS software 2.0 (AB Sciex). The other parameters on QSTAR-Elite were shown as follows: DP = 60, FP = 265, DP2 = 15, CAD = 5, IRD = 6, IRW = 5, curtain gas = 20, and ion spray voltage = 2000 V.

Two-dimensional (2D) LC/MS/MS

Tryptic digests of $CD4^+CD25^+CCR4^+$ T cells were dissolved in 10 mM ammonium formate in 25% acetonitrile and fractionated by a 0.2 × 250 mm monolith strong cation exchange column (GL Science, Tokyo, Japan). Peptides were eluted with an ammonium formate gradient from 10 mM to 1 M in curve = 3 mode for 70 minutes using a Prominence high-performance liquid chromatography (HPLC) system (Shimadzu Corporation, Kyoto, Japan). The eluate was fractionated into 20 fractions and analyzed individually by LTQ-Orbitrap-Velos mass spectrometer (Thermo Scientific, Bremen, Germany) accompanied with the Ultimate 3000 nano-HPLC system. The fractionated peptide samples were separated with the same gradient used in the QSTAR-Elite system described previously and analyzed by LTQ-Orbitrap-Velos acquiring a full MS scan on Fourier-transition mode with MS resolution = 60 000 and simultaneously MS/MS scans for the 20 most intense precursor ions in each MS spectrum on ion-trap mode with regular resolution. Other important parameters for LTQ-Orbitrap-Velos were as follows: capillary temp = 250, source voltage = 2 kV, MS scan range = mass-to-charge ratio (m/z) 400 to 1600, acquire data dependent CID MS/MS for top-20 intense precursors, and dynamic exclusion enabled during 30 seconds. For protein identification, all MS/MS spectra were searched against SwissProt database version 2012_06 (20 232 human protein sequences) using SEQUEST algorithm on ProteomeDiscoverer 1.3 software (Thermo Scientific) with the following parameters: MS tolerance = 3 ppm, MS/MS tolerance = 0.8 Da, maximum missed cleavages = 2, enzyme = trypsin, taxonomy = *Homo sapiens*, fixed modification = carbamidomethylation on cysteine, and variable modification = oxidation on methionine. We accepted the protein identification satisfying the false discovery rate $<1\%$ by Percolator false discovery rate estimation algorithm on ProteomeDiscoverer.

Label-free quantification analysis

The LC/MS/MS raw data were imported into the Expressionist RefinerMS module and subjected to the following data processing and relative quantification steps. The total work flow on the RefinerMS module is shown in supplemental Figure 1 (see the *Blood* Web site). The LC/MS/MS raw data set from 29 clinical samples was displayed in 2D planes (m/z vs retention time [RT]). The chromatogram grid was applied to all planes: scan counts = 10, polynom order = 3, and RT smoothing = 0. The planes were simplified by subtracting background noises using chromatogram chemical noise subtraction: RT window = 50 scans, quantile subtraction = 50%, and RT smoothing = 3 scans. After the noise subtraction, data points with intensity <10 were clipped to zero. The RT variety among 29 planes was adjusted by chromatogram RT alignment: RT transformation window = 0.2 minutes, RT search interval = 5 minutes, m/z window = 0.1 Da, and gap penalty = 1. Peaks were detected by chromatogram summed peak detection: summation window = 5 scans, overlap = 50, minimum peak size = 4 scans, maximum merge distance = 10 points, peak RT splitting = true, intensity profiling = max, gap/peak ratio = 1%, refinement threshold = 5, consistency threshold = 0.8, and signal/noise threshold = 1. The detected peaks were grouped into isotopic clusters derived from each molecule using 2-step chromatogram isotopic peak clustering. The first parameters were as follows: minimum charge = 1, maximum charge = 10, maximum missing peaks = 0, first allowed gap position = 3, RT window = 0.1 minute, m/z tolerance = 0.05 Da, isotope shape tolerance = 10, and minimum cluster size ration = 1.2. The second parameters were as follows: minimum charge = 1, maximum charge = 10, maximum missing peaks = 0, first allowed gap position = 3, RT window = 0.1 minute, m/z tolerance = 0.05 Da, and minimum cluster size ration = 0.6.

Expression vectors and siRNA

For the Δ_{19}CAN2 construct, the *CAPN2* fragment was amplified with primers 5′-CATGTCGACTCCCACGAGAGGGCCATCAAGT-3′ and 5′-CATTCTAGATCAAAGTACTGAGAAACAGAGCC-3′ from pBlueBacIII *CAPN2* and cloned into pEFBOS-Myc. Prior to the overexpression experiments, we confirmed that the sequence of the inserted *CAPN2* fragment was identical to the Mammalian Gene Collection sequence (accession number

From bloodjournal.hematologylibrary.org at ST MARIANNA SCHOOL on May 29, 2013. For personal use only.

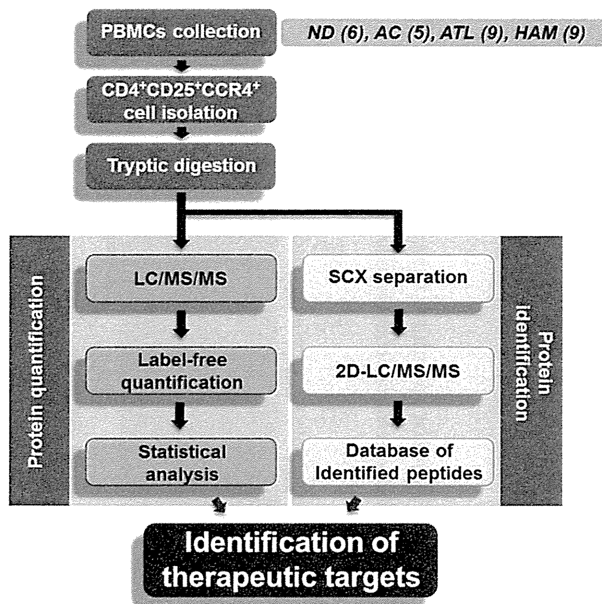

Figure 1. Schematic overview of proteomic profiling for $CD4^+CD25^+CCR4^+$ cells. PBMCs were collected from 6 normal donors, 5 asymptomatic carriers, 9 ATL patients, and 9 HAM/TSP patients, followed by isolation of the $CD4^+CD25^+CCR4^+$ subset using the cell-sorting system. The statistical candidate selection steps, including LC/MS/MS data processing, label-free quantification, and statistical analysis, were performed on the Expressionist proteome server. The protein identification database was separately established based on 2D LC/MS/MS analysis. ND, normal donors; AC, asymptomatic carriers.

BC021303). The 5-μg vector DNA was transfected to 1×10^6 cells. The small interfering RNAs (siRNAs) against *SPTAN1*, *PTMS*, *HSPE1*, and SHMT2 and siRNA universal negative control were purchased from Sigma-Aldrich. The 500-pmol siRNA oligo was transfected into 1×10^6 cells. The vectors and siRNAs were transfected into all cell lines except CCRF-CEM by Amaxa Nucleoportator transfection Kit V (Lonza, Cologne, Germany) and CCRF-CEM by Kit C (Lonza).

Cell cycle analysis and proliferation assay

For the cell cycle analysis, 1×10^5 to 2×10^5 cells were washed and agitated in 0.1% Triton-X (Sigma-Aldrich) with 100 ng/mL of ribonuclease (Sigma-Aldrich). Following addition of 1 μg/mL propidium iodide, the flow cytometric analysis was performed on FACScalibur (Becton Dickinson). The data analysis was performed using FlowJo software (Tree Star Inc., OR). Doublet events were eliminated from analyses by proper gating on FL2-W/FL2-A primary plots before histogram analysis of DNA content. Cell proliferation was estimated by measuring cell metabolic activity using Cell Counting Kit-8 (Dojindo, Kumamoto, Japan) following the manufacturer's recommendation.

Western blotting

Cells were lysed in lysis buffer [1% NP-40, 2 mM EGTA, 2 mM $MgCl_2$, 150 mM NaCl, 20 mM tris(hydroxymethyl)aminomethane–HCl (pH 7.5), 10% glycerol, containing the protease inhibitor cocktail Complete (Roche, IN)] and subjected to sodium dodecyl sulfate–polyacrylamide gel electrophoresis and transferred onto PVDF membranes. Following blocking with 4% Block Ace (Yukijirushi Nyugyo Inc., Tokyo, Japan), membranes were incubated with anti-myc (9E10; Sigma-Aldrich) or anti–α-II spectrin (Abcam, Cambridge, UK) antibodies. Membranes were then incubated with horseradish peroxidase–conjugated anti-mouse IgG (GE Healthcare, NJ) or anti-rabbit IgG (GE Healthcare), respectively, and visualized with Western Lightning kit (Perkin Elmer, MA).

Multiple reaction monitoring (MRM)

$CD4^+$ T cells were isolated from PBMCs using flow cytometry. The tryptic digests of the isolated cells were analyzed by 4000 Q-TRAP mass spectrometer (AB Sciex) accompanied with Ultimate 3000 nano-HPLC system. The LC gradient was as follows: 2% to 30% acetonitrile for 10 minutes and 30% to 95% acetonitrile for 5 minutes in 0.1% formic acid with a flow rate of 300 nL/min. The MRM transitions monitored were m/z 409.7/375.2 for α-II spectrin (SPTA2); m/z 538.3/889.5 for parathymosin (PTMS); m/z 507.3/147.1 for heat shock 10-kDa protein, mitochondrial (CH10); m/z 490.3/147.1 for serine hydroxymethyltransferase, mitochondrial (GLYM); and m/z 581.3/919.5 for β-actin, respectively. Individual peak areas were normalized by the peak area of β-actin. Data acquisition was performed with ion spray voltage = 2300 V, curtain gas = 10 psi, nebulizer gas = 10 psi, and an interface heating temperature = 150°C. The parameters were set as follows: declustering potential = 60, entrance potential = 10, collision cell exit potential = 10, and dwell time for each transition = 10 seconds. Collision energy was optimized to achieve maximum intensity for each MRM transition as follows: 34.03 V for m/z 409.7/175.1, 24.68 eV for m/z 538.3/889.5, 23.32 eV for m/z 507.3/147.1, 37.57 eV for m/z 490.3/147.1, and 31.58 eV for m/z 581.3/919.5.

Results

Quantitative proteome profiling of $CD4^+CD25^+CCR4^+$ T cells

A schematic overview of the screening approach is shown in Figure 1. To identify diagnostic markers expressed in HTLV-1–infected T cells, a $CD4^+CD25^+CCR4^+$ subset of PBMCs from 6 uninfected volunteers, 5 asymptomatic carriers, 9 HAM/TSP patients, and 9 ATL patients was isolated by flow cytometry (Figure 2). The averaged proportion of $CD4^+CD25^+CCR4^+$ cells in $CD4^+$ T cells from 4 clinical groups was 6.48 ± 2.46%, 13.17 ± 13.06%, 20.55 ± 10.73%, and 55.83 ± 22.40%, respectively, indicating that the occupancy of viral reservoir cells varied drastically among both pathological groups and even individuals within a group. Enrichment of the infected cells was confirmed by viral load measurement of the used samples (supplemental Figure 2). As reported previously,[10] the viral load of $CD4^+CD25^+CCR4^+$ cells (37.91 copies/100 cells on average) was ~10 times higher than that of $CD4^+CD25^-CCR4^-$ cells (4.12 copies/100 cells on average), indicating that the former cells were evidently the HTLV-1–enriched fraction. This fact strongly supports the importance of

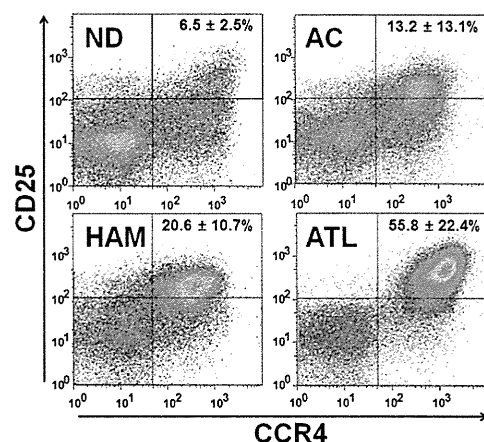

Figure 2. Representative sorting results of $CD4^+CD25^+CCR4^+$ cells. After labeling with anti-CD3-FITC, anti-CD4-Cy7, anti-CD25-APC, and anti-CCR4-PE, the $CD3^+CD4^+CD25^+CCR4^+$ fraction was isolated. The averaged content ± standard deviation (%) of $CD25^+CCR4^+$ cells out of $CD3^+CD4^+$ cells was calculated for each clinical group and is displayed in the upper right section of the panels.

From bloodjournal.hematologylibrary.org at ST MARIANNA SCHOOL on May 29, 2013. For personal use only.

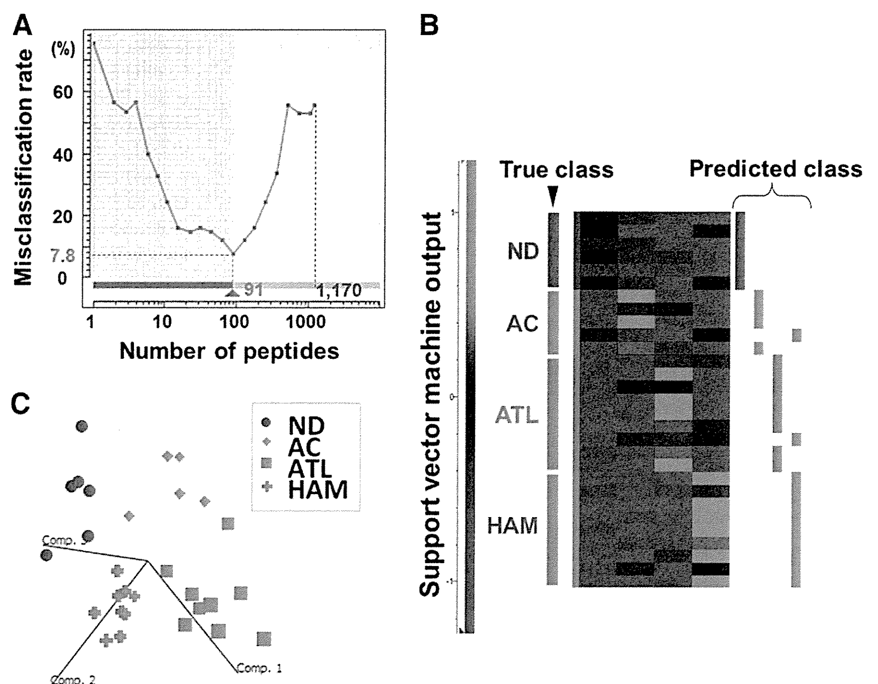

Figure 3. Statistical extraction of candidate therapeutic targets. The 14 064 nonredundant peptides detected were subjected to a 4-group Kruskal-Wallis test (ND, AC, ATL, and HAM), resulting in identification of 1170 first candidates ($P < .01$). ND, normal donors; AC, asymptomatic carriers. (A) Next, the Expressionist ranking method further narrowed down the candidates to 91 peptides based on SVM-REF so that the misclassification rate in the cross-validation test became minimum, 7.8%. (B) The predicted classification result by leave-one-out cross-validation test. The 27 out of 29 cases were successfully classified into the true classes. (C) The three-dimensional plot shows the additional assessment for the classification power of 91 classifiers by principal component analysis. Comp. 1 to 3 indicate principal components 1 to 3.

enriching pathogenic cells for rigorous quantitative biomarker discovery.

An accurately adjusted number of $CD4^+CD25^+CCR4^+$ cells from 29 cases were digested with trypsin and subjected to LC/MS/MS analysis individually. Because recent mass spectrometers often deal with data on the order of hundreds of megabytes per sample, it has been considered almost impossible to calculate a data set larger than a gigabyte from large-scale clinical samples on desktop computers. Hence, we constructed a proteomics server equipped with a 12-core central processing unit, 36 SAS hard disks, and 192-GB physical memories driving the Expressionist, which was designed to combine the database module, the data processing module, and the statistical analysis module into a single integrative platform for genomics, proteomics, and metabolomics. The detailed work flow for data processing and quantification for 29 LC/MS/MS raw data was described in the "Materials and methods" and is illustrated in supplemental Figure 1. Finally, 68 454 nonredundant peaks were detected and grouped into 37 143 isotopic clusters, or molecules. As tryptic peptides should appear as multivalent ions in electrospray ionization mass spectra, 23 079 singly charged ions were removed, resulting in utilization of 14 064 peptide signals for further statistical selection of diagnostic markers.

Statistical identification of candidate diagnostic markers for ATL

A stepwise statistical extraction was employed for the effective identification of proteins, which demonstrated specific up- or downregulation in the ATL group. In the first stage, a 4-group Kruskal-Wallis test was performed to roughly extract the candidates showing a significantly distinct expression level among 4 clinical groups. Here we set the cutoff line at $P < .01$ and obtained 1170 first candidate peptides simply because the isolated peptide set using this criterion showed the best performance in the following prediction model.

Next, we selected the final candidates by the support vector machine–recursive feature elimination algorithm in the Expressionist Analyst module. Support vector machine–recursive feature elimination is a candidate elimination method based on SVM, which enabled us to improve the classification outputs by selecting the best-performing peptide set among initially provided candidates.[11] As a result, a combination of 91 peptides showed the lowest misclassification rate (7.78%) in a leave-one-out cross-validation test (Figure 3A-B). To evaluate the classification efficiency of 91 selected candidates, the principal component analysis was performed. Figure 3C shows the three-dimensional plot of 29 clinical samples based on the 3 best-explainable components, which illustrated statistically clear segregation among the 4 clinical groups. These assessments indicated that the 91 peptides should be a sufficient set of classifiers that closely associated with the pathological characteristics of the 4 clinical groups.

Based on an independently constructed 6279-protein identification database for $CD4^+CD25^+CCR4^+$ cells using 2D LC/MS/MS (see details in "Materials and methods"), 19 peptides among the 91 candidate peptides were successfully assigned to 17 proteins listed in Table 1. The mass spectrometric quantification profiles for the 19 peptides are also shown in Figure 4 (box plots).

Recovering CAN2 activity induced cell death in ATL cells

Our diagnostic marker discovery for ATL identified an enzyme-substrate pair, CAN2 and SPTA2, which demonstrated significantly aberrant expression level in ATL patients (Figure 4). Interestingly, the intensities of the 2 proteins in 27 screening cases (without 2 statistical outliers in Figure 4) showed a clearly inverse correlation ($R^2 = 0.395$, Figure 5A). To examine whether CAN2 downregulation and/or SPTA2 upregulation might be essential for the growth of ATL cells, the enzymatic activity of CAN2 was rescued by overexpressing the constitutively active form of CAN2 (Δ_{19}CAN2) in 3 ATL cell lines, SO-4, KOB, and KK1. After 36 hours of transfection, significant inhibition of cell proliferation (Figure 5B) and induction of sub-G1 transition was observed by activation of CAN2 in 3 ATL cells, but not in 4 non-ATL leukemia cell lines (Figure 5C). Furthermore, overexpression of Δ_{19}CAN2 drastically attenuated the expression level of SPTA2 in the ATL cell

From bloodjournal.hematologylibrary.org at ST MARIANNA SCHOOL on May 29, 2013. For personal use only.

Table 1. List of 17 protein classifiers for categorization of normal donors, asymptomatic carriers, HAM/TSP, and ATL

Accession	Protein name	*P* value (Kruskal-Wallis test)	m/z	RT	Charge	Peptide score	Identity or homology threshold	Sequence
LPPL	Eosinophil lysophospholipase	2.3.E-03	409.722	47.4	2	36.3	27	MVQVWR
CH10	Heat shock 10-kDa protein, mitochondrial	2.5.E-03	430.721	40.6	2	26.2	21	GGIMLPEK
PRG2	Bone marrow proteoglycan	2.4.E-03	528.271	64.6	2	31.6	28	RLPFICSY
MOES	Moesin	8.1.E-04	532.253	26.8	2	46.2	29	EKEELMER
MNDA	Myeloid cell nuclear differentiation antigen	9.4.E-03	647.863	69.1	2	67.3	24	SLLAYDLGLTTK
GLYM	Serine hydroxymethyltransferase, mitochondrial	8.7.E-04	408.551	21.6	3	31.1	18	HADIVTTTTHK
PTMS	Parathymosin	9.7.E-04	453.875	17.8	3	41.2	25	AAEEEDEADPKR
TPIS	Triosephosphate isomerase	9.1.E-03	472.266	71.0	3	54.0	28	QSLGELIGTLNAAK
HSP71	Heat shock 70-kDa protein 1A/1B	9.7.E-03	563.307	65.5	3	93.8	21	IINEPTAAAIAYGLDR
CD6	T-cell differentiation antigen CD6	7.7.E-03	592.306	37.8	3	62.7	22	VLCQSLGCGTAVERPK
ANXA1	Annexin A1	4.4.E-04	612.347	61.5	3	57.0	17	RKGTDVNVFNTILTTR
ANXA6	Annexin A6	2.3.E-03	669.017	70.9	3	54.7	16	AMEGAGTDEKALIEILATR
SPTA2	Spectrin α chain, brain	5.4.E-03	409.718	28.8	2	42.7	30	EAGSVSLR
GLYM	Serine hydroxymethyltransferase, mitochondrial	1.1.E-03	428.240	57.0	2	42.8	27	SGLIFYR
DRB1s	HLA class II histocompatibility antigen, DRB1-1, 4, 10, 11, 13, 15, 16 β chain	1.0.E-02	478.216	25.8	2	55.9	25	AAVDTYCR
CAN2	Calpain-2 catalytic subunit	2.4.E-03	483.253	54.0	2	66.6	29	SDTFINLR
STAT1	Signal transducer and activator of transcription 1-α/β	7.3.E-03	486.290	21.7	2	39.1	29	KILENAQR
PRG2	Bone marrow proteoglycan	9.4.E-04	497.742	49.2	2	31.6	27	FQWVDGSR
CXCL7	Platelet basic protein	1.3.E-03	528.761	43.1	2	51.7	28	ICLDPDAPR

line SO-4 (Figure 5D), but not in the non-ATL leukemia cell line Jurkat (Figure 5E). On the other hand, an additional cell proliferation assay using siRNA against *SPTAN1* revealed that reduction of SPTA2 was not sufficient for the induction of cell death for ATL cells (supplemental Figures 3 and 4).

In addition, 3 proteins (PTMS, CH10, and GLYM) were also found to be upregulated in ATL cells. To address the roles of these proteins, a cell proliferation assay was conducted using 3 ATL cell lines treated with siRNAs against *PTMS*, *HSPE1* (gene symbol of CH10), or *SHMT2* (gene symbol of GLYM) (supplemental Figure 4). As a result, suppression of the *SHMT2* gene induced significant growth inhibition for all 3 ATL cell lines. Although si*HSPE1*-treated KOB cells showed a statistically significant decrease in cell growth rate, si*HSPE1* and si*PTMS* had only partial

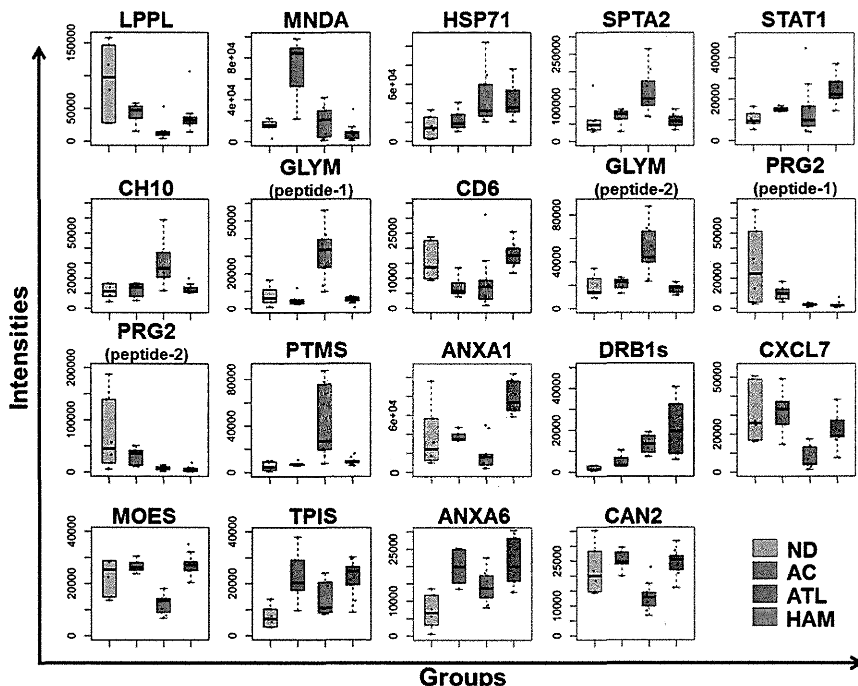

Figure 4. Summary of quantitative features for the 17 protein classifiers identified. The 19 box plots (see Table 1 for protein names) show the results of mass spectrometric quantification and protein identification. We finally identified 19 peptides out of 91 candidates in Figure 3, which were assigned to 17 proteins. Proteins identified from 2 distinct peptides were shown as GLYM (peptides 1 and 2) or PRG2 (peptides 1 and 2). The y-axis indicates normalized relative intensity of peptides in mass spectrometric data. ND, normal donors; AC, asymptomatic carriers.

From bloodjournal.hematologylibrary.org at ST MARIANNA SCHOOL on May 29, 2013. For personal use only.

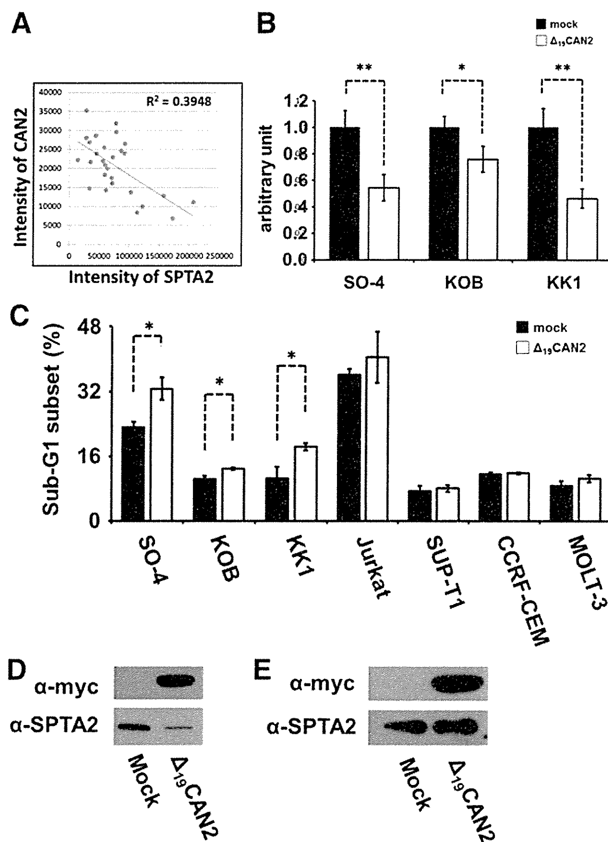

Figure 5. Rescue of CAN2 activity induced cell death in ATL cells. (A) Correlation between CAN2 and SPTA2 expression level in 27 cases. (B) Cell proliferation was measured by MTT assay on SO-4, KOB, and KK1 cells 36 hours after transfection of mock vector or Δ_{19}CAN2. **P* < .05; ***P* < .01 by Student *t* test. (C) Overexpression of Δ_{19}CAN2 significantly accelerated cell death in 3 ATL (SO-4, KOB, and KK1) and 4 non-ATL (Jurkat, SUP-T1, CCRF-CEM, and MOLT-3) cell lines. ***P* < .05 by Student *t* test. The drastic attenuation of SPTA2 expression was observed after transfection of Δ_{19}CAN2 in SO-4 cells (D), but not in Jurkat cells (E). The immunoblot of anti-myc tag confirmed the expression of exogenous Δ_{19}CAN2.

or no effects on proliferation of ATL cell lines. To further confirm whether the overexpression of SPTA2, PTMS, CH10, or GLYM protein would be an ATL-specific molecular signature, the expression levels of these proteins in 8 clinical samples were evaluated by the mass spectrometric quantification technology MRM (supplemental Figures 5 and 6). Expression of SPTA2, GLYM, and CH10 in cells derived from ATL patients was significantly higher than that in cells derived from HAM/TSP patients. The level of PTMS also showed a clearly increasing tendency in the ATL patient group. Taken together, these results suggested that the deprivation of CAN2 activity and upregulation of GLYM in HTLV-1–infected T cells might have a key role at the onset or progression of ATL.

Discussion

In the past decade, proteomics technologies have developed dramatically for the purpose of obtaining more and more comprehensive and sensitive proteome maps in cells or clinical specimens. The performance of mass spectrometers in particular has exhibited remarkable progress; however, as for sensitivity and throughput, it has still been difficult to identify biomarkers from crude samples including body fluids or total cell lysate. A major reason could be that the range of protein concentration in the analyte is indeed much larger than the dynamic range of recent mass spectrometers.[12] The other essential factor to be improved for clinical proteomics is the capacity of the bioinformatics platform to allow analysis of a sufficient number of clinical samples in order to statistically overcome the significant individual variability.[13]

Concerning the first issue, we previously developed and applied various focused proteomic applications targeting molecular biochemical features including glycan structure biomarkers[14-16] and low-molecular-weight peptide biomarkers.[17] The preenrichment of subproteome fractions effectively reduces the complexity of crude samples and allowed us to identify potential serum cancer biomarkers successfully. Through our previous knowledge, we provide an approach for investigating infectious diseases by employing virus-infected cell-focused proteomics. In addition to HTLV-1, for instance, isolation of HIV-infected cells is highly desired because the frequency of these cells in AIDS patients' PBMCs is ~1 out of 10^4 to 10^5 cells.[18] Actually, we successfully demonstrated the effect of HTLV-1–infected cell isolation on the elimination of individual variability (Figure 2, supplemental Figure 2) and reliable identification of disease state–associated proteins (Figures 4 and 5). We further showed the potential of the next-generation bioinformatics platform Expressionist to remove the constraint on the capacity of data size acquired from high-end mass spectrometers. Expressionist covered whole discovery steps from processing of raw mass spectrometer data to statistical analyses (Figures 1 and 3, and supplemental Figure 1) and, importantly, could perform quantification analysis using a basically unlimited number of clinical samples. Hence, in parallel with the development of mass spectrometers, high-specification and inexpensive OMICS server systems are necessary for future diagnostic marker and therapeutic target discoveries using hundreds or thousands of clinical specimens.

In this study, we focused on the $CD4^+CD25^+CCR4^+$ T-cell subpopulation in which T helper 2, T helper 17, and regulatory T (Treg) cells were mainly involved.[10] The purpose for which we used this subset was to technically enrich the preferential viral reservoir cells and to strengthen reliability of screening results. However, investigating proteome behaviors of these subtypes in HTLV-1–associated diseases is also important physiologically because it has been frequently reported that deregulated Treg plays significant roles in pathogenesis of ATL and HAM/TSP. Indeed, aberrant proliferation of Treg cells is considered the main cause of immunodeficiency in ATL patients because of their innate immunosuppressive functions,[19] whereas abnormal production of interferon γ from infected Treg cells might induce chronic spinal inflammation in HAM/TSP patients.[20] Given the list of our 17 classifier proteins, activation of signal transducer and activator of transcription 1-α/β is the well-known key factor for HAM/TSP,[21] whereas upregulation of heat shock 70-kDa protein 1A/1B, CH10, and PTMS were reported in many other types of tumors.[22-24] The association of these 4 proteins with the etiology of HAM/TSP and ATL would be evident according to the previous work, supporting that our other candidates might similarly have a direct impact on the transformation of Treg cells after infection of HTLV-1. Particularly, the specific upregulation of GLYM in ATL cells represents the first evidence that excessive folate metabolism might be essential for the progression or survival of ATL cells because GLYM is a fundamental enzyme catalyzing the supply of glycine accompanying the conversion of tetrahydrofolate to 5,10-methylenetetrahydrofolate.[25] Indeed, the suppression of GLYM expression, which was confirmed to be upregulated in ATL patients, resulted in significant reduction of cell growth. This observation suggests that diminishing GLYM

From bloodjournal.hematologylibrary.org at ST MARIANNA SCHOOL on May 29, 2013. For personal use only.

expression or enzyme activity could be a promising strategy for molecular-targeting treatment of ATL. Together with the downregulation of CAN2 in the ATL cells shown in Figure 5, the proteins listed in Table 1 could provide the molecular basis for not only interpretation of physiological mechanisms in ATL or HAM/TSP but also development of novel therapeutic agents for HTLV-1–associated diseases.

CAN2 belongs to a Ca^{2+}-regulated cytosolic cysteine protease family, which includes 14 calpain isoforms.[26] The enzymatic activity of calpain is implicated in diverse physiological processes, such as cytoskeletal remodeling, cellular signaling, and apoptosis.[26] As an example of a spectrin-mediated apoptosis pathway, it was reported that CAN2 produced SPTA2 breakdown products following traumatic brain injury.[27] Because SPTA2 interacts with calmodulin and constructs the membrane cytoskeletons, its breakdown is considered a process of membrane structural changes during cell death.[28,29] This fact is concordant with our finding in ATL, suggesting that accumulation of SPTA2 in ATL cells can be attributed to the suppression of CAN2 expression and contribute to circumvent apoptosis. In the analysis of basal levels of CAN2 and SPTA2 in 7 cell lines (supplemental Figure 7), 3 ATL cell lines showed endogenous expression of CAN2 and moderate levels of SPTA2. On the other hand, 4 non-ATL leukemia cells demonstrated very high expression of SPTA2 and undetectable levels of CAN2. Although we found the downregulation of CAN2 and accumulation of SPTA2 in ATL cells, this tendency might be more distinctive in HTLV-1 (–) leukemia cells. Taken together, even though the expression level of CAN2 was indeed suppressed in ATL cells, the CAN2-SPTA2 apoptotic pathway itself might remain normal. In contrast, this pathway was considered to be impaired at multiple stages in HTLV-1 (–) leukemia cells because CAN2 expression was completely diminished (supplemental Figure 7) and overexpression of CAN2 could not reactivate the CAN2-SPTA2 apoptotic pathway (Figure 5B-E). In these cells, not only genetic downregulation of CAN2 but also inhibition of CAN2 enzymatic activity might be involved in the carcinogenesis.

In conclusion, comprehensive proteomic profiling of HTLV-1–infected T cells provided 17 disease-associated signature proteins, which have great potential for future clinical use as diagnostic biomarkers. As we described regarding the relationship between the CAN2-SPTA2 pathway and ATL phenotypes, further individual functional analyses will contribute to understanding the detailed molecular mechanisms involved in the onset or progression of HAM/TSP and ATL.

Acknowledgments

The authors thank Dr Hiroyuki Sorimachi for kindly providing pBlueBacIIICAPN2 vector.

This work was supported by Research on Measures for Intractable Diseases, the Ministry of Health Labour and Welfare Japan.

Authorship

Contribution: M.I. and K.U. designed the study, performed experiments, analyzed results, and wrote the manuscript; A.T. and N.S. performed experiments; N.A., T.S., A.U., and Y.Y. collected the clinical samples and performed flow cytometric experiments; Y.N. and H.N. revised the manuscript; and all authors discussed the results and commented on the manuscript.

Conflict-of-interest disclosure: The authors declare no competing financial interests.

Correspondence: Koji Ueda, Laboratory for Biomarker Development, Center for Genomic Medicine, RIKEN, General Research Building 6F, Institute of Medical Science, 4-6-1 Shirokanedai, Minato-ku, Tokyo, Japan, 1088639; e-mail: k-ueda@riken.jp.

References

1. Yamashita M, Ido E, Miura T, Hayami M. Molecular epidemiology of HTLV-I in the world. *J Acquir Immune Defic Syndr Hum Retrovirol.* 1996;13(suppl 1):S124-S131.
2. Asquith B, Zhang Y, Mosley AJ, et al. In vivo T lymphocyte dynamics in humans and the impact of human T-lymphotropic virus 1 infection. *Proc Natl Acad Sci U S A.* 2007;104(19):8035-8040.
3. Sakashita A, Hattori T, Miller CW, et al. Mutations of the p53 gene in adult T-cell leukemia. *Blood.* 1992;79(2):477-480.
4. Beltran B, Quiñones P, Morales D, Cotrina E, Castillo JJ. Different prognostic factors for survival in acute and lymphomatous adult T-cell leukemia/lymphoma. *Leuk Res.* 2011;35(3):334-339.
5. Ishida T, Joh T, Uike N, et al. Defucosylated anti-CCR4 monoclonal antibody (KW-0761) for relapsed adult T-cell leukemia-lymphoma: a multicenter phase II study. *J Clin Oncol.* 2012;30(8):837-842.
6. Semmes OJ, Cazares LH, Ward MD, et al. Discrete serum protein signatures discriminate between human retrovirus-associated hematologic and neurologic disease. *Leukemia.* 2005;19(7):1229-1238.
7. Kirk PD, Witkover A, Courtney A, et al. Plasma proteome analysis in HTLV-1-associated myelopathy/tropical spastic paraparesis. *Retrovirology.* 2011;8:81.
8. Rahman S, Quann K, Pandya D, Singh S, Khan ZK, Jain P. HTLV-1 Tax mediated downregulation of miRNAs associated with chromatin remodeling factors in T cells with stably integrated viral promoter. *PLoS ONE.* 2012;7(4):e34490.
9. Polakowski N, Gregory H, Mesnard JM, Lemasson I. Expression of a protein involved in bone resorption, Dkk1, is activated by HTLV-1 bZIP factor through its activation domain. *Retrovirology.* 2010;7:61.
10. Yamano Y, Araya N, Sato T, et al. Abnormally high levels of virus-infected IFN-gamma+ CCR4+ CD4+ CD25+ T cells in a retrovirus-associated neuroinflammatory disorder. *PLoS ONE.* 2009;4(8):e6517.
11. Oh JH, Gao J, Nandi A, Gurnani P, Knowles L, Schorge J. Diagnosis of early relapse in ovarian cancer using serum proteomic profiling. *Genome Inform.* 2005;16(2):195-204.
12. Anderson NL, Anderson NG. The human plasma proteome: history, character, and diagnostic prospects. *Mol Cell Proteomics.* 2002;1(11):845-867.
13. Nordon IM, Brar R, Hinchliffe RJ, Cockerill G, Thompson MM. Proteomics and pitfalls in the search for potential biomarkers of abdominal aortic aneurysms. *Vascular.* 2010;18(5):264-268.
14. Ueda K, Katagiri T, Shimada T, et al. Comparative profiling of serum glycoproteome by sequential purification of glycoproteins and 2-nitrobenzensulfenyl (NBS) stable isotope labeling: a new approach for the novel biomarker discovery for cancer. *J Proteome Res.* 2007;6(9):3475-3483.
15. Ueda K, Fukase Y, Katagiri T, et al. Targeted serum glycoproteomics for the discovery of lung cancer-associated glycosylation disorders using lectin-coupled ProteinChip arrays. *Proteomics.* 2009;9(8):2182-2192.
16. Ueda K, Takami S, Saichi N, et al. Development of serum glycoproteomic profiling technique; simultaneous identification of glycosylation sites and site-specific quantification of glycan structure changes. *Mol Cell Proteomics.* 2010;9(9):1819-1828.
17. Ueda K, Saichi N, Takami S, et al. A comprehensive peptidome profiling technology for the identification of early detection biomarkers for lung adenocarcinoma. *PLoS ONE.* 2011;6(4):e18567.
18. Bahbouhi B, al-Harthi L. Enriching for HIV-infected cells using anti-gp41 antibodies indirectly conjugated to magnetic microbeads. *Biotechniques.* 2004;36(1):139-147.
19. Matsubar Y, Hori T, Morita R, Sakaguchi S, Uchiyama T. Delineation of immunoregulatory properties of adult T-cell leukemia cells. *Int J Hematol.* 2006;84(1):63-69.
20. Best I, López G, Verdonck K, et al. IFN-gamma production in response to Tax 161-233, and frequency of CD4+ Foxp3+ and Lin HLA-

From bloodjournal.hematologylibrary.org at ST MARIANNA SCHOOL on May 29, 2013. For personal use only.

DRhigh CD123+ cells, discriminate HAM/TSP patients from asymptomatic HTLV-1-carriers in a Peruvian population. *Immunology.* 2009; 128(1, pt 2):e777-e786.

21. Nakamura N, Fujii M, Tsukahara T, et al. Human T-cell leukemia virus type 1 Tax protein induces the expression of STAT1 and STAT5 genes in T-cells. *Oncogene.* 1999;18(17): 2667-2675.
22. Alaiya AA, Al-Mohanna M, Aslam M, et al. Proteomics-based signature for human benign prostate hyperplasia and prostate adenocarcinoma. *Int J Oncol.* 2011;38(4): 1047-1057.
23. Cappello F, Rappa F, David S, Anzalone R, Zummo G. Immunohistochemical evaluation of PCNA, p53, HSP60, HSP10 and MUC-2 presence and expression in prostate carcinogenesis. *Anticancer Res.* 2003;23(2B): 1325-1331.
24. Letsas KP, Vartholomatos G, Tsepi C, Tsatsoulis A, Frangou-Lazaridis M. Fine-needle aspiration biopsy-RT-PCR expression analysis of prothymosin alpha and parathymosin in thyroid: novel proliferation markers? *Neoplasma.* 2007; 54(1):57-62.
25. Anderson DD, Quintero CM, Stover PJ. Identification of a de novo thymidylate biosynthesis pathway in mammalian mitochondria. *Proc Natl Acad Sci USA.* 2011;108(37): 15163-15168.
26. Storr SJ, Carragher NO, Frame MC, Parr T, Martin SG. The calpain system and cancer. *Nat Rev Cancer.* 2011;11(5):364-374.
27. Liu MC, Akle V, Zheng W, et al. Comparing calpain- and caspase-3-mediated degradation patterns in traumatic brain injury by differential proteome analysis. *Biochem J.* 2006;394(pt 3): 715-725.
28. Wallis CJ, Wenegieme EF, Babitch JA. Characterization of calcium binding to brain spectrin. *J Biol Chem.* 1992;267(7): 4333-4337.
29. Liu X, Van Vleet T, Schnellmann RG. The role of calpain in oncotic cell death. *Annu Rev Pharmacol Toxicol.* 2004;44: 349-370.

CSF CXCL10, CXCL9, and Neopterin as Candidate Prognostic Biomarkers for HTLV-1-Associated Myelopathy/Tropical Spastic Paraparesis

Tomoo Sato[1], Ariella Coler-Reilly[1], Atae Utsunomiya[2], Natsumi Araya[1], Naoko Yagishita[1], Hitoshi Ando[1], Junji Yamauchi[1], Eisuke Inoue[3], Takahiko Ueno[4], Yasuhiro Hasegawa[5], Kusuki Nishioka[6], Toshihiro Nakajima[6,7], Steven Jacobson[8], Shuji Izumo[9], Yoshihisa Yamano[1]*

1 Department of Rare Diseases Research, Institute of Medical Science, St. Marianna University School of Medicine, Kawasaki, Kanagawa, Japan, 2 Department of Hematology, Imamura Bun-in Hospital, Kagoshima, Japan, 3 Department of Biostatistics, School of Pharmacy, Kitasato University, Tokyo, Japan, 4 Unit of Medical Statistics, St. Marianna University School of Medicine, Kawasaki, Kanagawa, Japan, 5 Division of Neurology, Department of Internal Medicine, St. Marianna University School of Medicine, Kawasaki, Kanagawa, Japan, 6 Institute of Medical Science, Tokyo Medical University, Tokyo, Japan, 7 Department of Biomedical Engineering, Osaka Institute of Technology, Osaka, Japan, 8 Viral Immunology Section, Neuroimmunology Branch, National Institutes of Health, Bethesda, Maryland, United States of America, 9 Molecular Pathology, Center for Chronic Viral Diseases, Kagoshima University, Kagoshima, Japan

Abstract

Background: Human T-lymphotropic virus type 1 (HTLV-1) -associated myelopathy/tropical spastic paraparesis (HAM/TSP) is a rare chronic neuroinflammatory disease. Since the disease course of HAM/TSP varies among patients, there is a dire need for biomarkers capable of predicting the rate of disease progression. However, there have been no studies to date that have compared the prognostic values of multiple potential biomarkers for HAM/TSP.

Methodology/Principal Findings: Peripheral blood and cerebrospinal fluid (CSF) samples from HAM/TSP patients and HTLV-1-infected control subjects were obtained and tested retrospectively for several potential biomarkers, including chemokines and other cytokines, and nine optimal candidates were selected based on receiver operating characteristic (ROC) analysis. Next, we evaluated the relationship between these candidates and the rate of disease progression in HAM/TSP patients, beginning with a first cohort of 30 patients (Training Set) and proceeding to a second cohort of 23 patients (Test Set). We defined "deteriorating HAM/TSP" as distinctly worsening function (≥3 grades on Osame's Motor Disability Score (OMDS)) over four years and "stable HAM/TSP" as unchanged or only slightly worsened function (1 grade on OMDS) over four years, and we compared the levels of the candidate biomarkers in patients divided into these two groups. The CSF levels of chemokine (C-X-C motif) ligand 10 (CXCL10), CXCL9, and neopterin were well-correlated with disease progression, better even than HTLV-1 proviral load in PBMCs. Importantly, these results were validated using the Test Set.

Conclusions/Significance: As the CSF levels of CXCL10, CXCL9, and neopterin were the most strongly correlated with rate of disease progression, they represent the most viable candidates for HAM/TSP prognostic biomarkers. The identification of effective prognostic biomarkers could lead to earlier detection of high-risk patients, more patient-specific treatment options, and more productive clinical trials.

Citation: Sato T, Coler-Reilly A, Utsunomiya A, Araya N, Yagishita N, et al. (2013) CSF CXCL10, CXCL9, and Neopterin as Candidate Prognostic Biomarkers for HTLV-1-Associated Myelopathy/Tropical Spastic Paraparesis. PLoS Negl Trop Dis 7(10): e2479. doi:10.1371/journal.pntd.0002479

Editor: Joseph Raymond Zunt, University of Washington, United States of America

Received January 18, 2013; **Accepted** September 2, 2013; **Published** October 10, 2013

This is an open-access article, free of all copyright, and may be freely reproduced, distributed, transmitted, modified, built upon, or otherwise used by anyone for any lawful purpose. The work is made available under the Creative Commons CC0 public domain dedication.

Funding: This work was supported by the "Research on Measures for Intractable Diseases" Project of the Ministry of Health, Labour, and Welfare, the MEXT-Supported Program for the Strategic Research Foundation at Private Universities, 2008–2012, the Grant-in-Aid for Scientific Research from the Ministry of Education, Culture, Sports, Science and Technology, and the Takeda Science Foundation. The funders had no role in study design, data collection or analysis, decision to publish, or preparation of the manuscript.

Competing Interests: The authors have declared that no competing interests exist.

* E-mail: yyamano@marianna-u.ac.jp

Introduction

Human T-lymphotropic virus type 1 (HTLV-1) is a human retrovirus associated with persistent infection of T-cells [1]. While the majority of HTLV-1-infected individuals remain asymptomatic, approximately 2.5–5% develop an aggressive T-cell malignancy, termed adult T-cell leukemia (ATL) [2,3] and 0.3–3.8% develop a serious chronic neuroinflammatory disease, termed HTLV-1-associated myelopathy/tropical spastic paraparesis (HAM/TSP) [4–6]. Aside from Japan, endemic areas for this virus and the associated disorders are mostly located in developing countries in the Caribbean, South America, Africa, the Middle East, and Melanesia [7,8], which may explain why these conditions have remained ill-defined and virtually untreatable for so long [9].

HAM/TSP is characterized by unremitting myelopathic symptoms such as spastic paraparesis, lower limb sensory disturbance, and bladder/bowel dysfunction [10,11]. Although

Author Summary

HTLV-1-associated myelopathy/tropical spastic paraparesis (HAM/TSP) is a rare neurodegenerative disease caused by infection with human T-lymphotropic virus type 1 (HTLV-1). HTLV-1 infects 10–20 million people worldwide, and, depending on the region, 0.25–3.8% of infected individuals develop HAM/TSP. As the disease progresses, chronic inflammation damages the spinal cord and lower limb and bladder function gradually decline. In the worst cases, even middle-aged patients can become perpetually bedridden. Today, there are treatments that may alleviate the symptoms to a certain degree, but there is no cure that can halt disease progression, and there are no known biomarkers to indicate the level and speed of disease progression. In this study, we successfully identified three promising candidate biomarkers. We believe that the use of these biomarkers could lead to more accurate prognoses and more prudent, patient-specific treatment plans. We not only hope that these biomarkers are sensitive enough to use as selection criteria for clinical trials, but also that measurements of these biomarkers can be used to accurately evaluate drug effectiveness. In short, the biomarkers we identified have the potential to help more effectively treat current HAM/TSP patients and to pave the way for new drugs to potentially cure future HAM/TSP patients.

the symptoms of HAM/TSP have been well documented for quite some time, the rate at which these symptoms progress has only recently become a point of interest. The clinical course of HAM/TSP has classically been described very simply as insidious onset and continuous progression [12], but recent reports have hinted at a more complex, heterogeneous pool of patients with differing clinical needs. Recent studies have shown that although HAM/TSP usually progresses slowly and without remission as per the classical description, there is a subgroup of patients whose conditions decline unusually quickly and who may be unable to walk within two years of onset and another subgroup whose conditions decline unusually slowly and who may only display very mild symptoms [13–15]. It is only logical that these patients should receive treatments tailored to suit their individual needs rather than identically aggressive treatments. Unfortunately, clinicians are currently only able to distinguish between these different groups by observing the way a patient's disease progresses over time, usually years; clinicians often decide to treat the patients immediately and identically rather than wait and allow the disease to progress further. Therein lies the dire need for biomarkers with the power to forecast the rate and extent of disease progression and enable clinicians to make more accurate prognoses and prescribe the most appropriate and effective treatments in a timely manner.

Several candidate prognostic biomarkers with elevated levels in HAM/TSP patients have already been identified in the peripheral blood and cerebrospinal fluid (CSF). In the peripheral blood, such candidates include the HTLV-1 proviral load in peripheral blood mononuclear cells (PBMCs) and serum levels of the soluble IL-2 receptor (sIL-2R) [16,17]. The level of neopterin in the CSF has been reported to be a useful parameter for detecting cell-mediated immune responses in the spinal cord of HAM/TSP patients and the CSF anti-HTLV-1 antibody titer has been shown to be associated both with CSF neopterin levels and the severity of clinical symptoms [18–20]. In addition, several cytokines have been detected in the CSF and/or spinal cord of HAM/TSP patients, including interleukin (IL)-1β, granulocyte-macrophage colony-stimulating factor (GM-CSF), interferon (IFN)-γ, and tumor necrosis factor (TNF)-α [21–24]. Some chemokines, such as chemokine (C-X-C motif) ligand (CXCL) 9, CXCL10, and chemokine (C-C motif) ligand (CCL) 5, have been shown to be substantially elevated in both the blood and the CSF with respect to asymptomatic carriers (ACs) or patients with other neurological diseases such as multiple sclerosis [25–28]. This is the first study to compare the adequacies of several of these candidate biomarkers for forecasting the rate of disease progression.

We hypothesized the existence of biomarkers capable of differentiating stable and deteriorating HAM/TSP patients. In this retrospective study, a preliminary experiment was first conducted to select the most promising candidate biomarkers by comparing blood and CSF levels in HAM/TSP patients and control subjects (Figure S1). Four candidate blood markers (sIL-2R, CXCL9, CXCL10, and proviral load) and five candidate CSF markers (CXCL9, CXCL10, neopterin, cell count, and anti-HTLV-1 antibody titer) were selected. To evaluate the relative effectiveness of these candidate biomarkers for predicting rate of disease progression, a classification system was created and HAM/TSP patients were designated as either deteriorating or relatively stable. The levels of candidate biomarkers were then compared between the two patient groups. In the current study, we identified three viable candidates for HAM/TSP prognostic biomarkers that could lead to more accurate prognoses and more prudent, patient-specific treatment plans.

Materials and Methods

Ethical considerations

The study was designed and conducted in accordance with the tenets of the Declaration of Helsinki. The protocol in this study was approved by the Ethics Review Committee of St. Marianna University School of Medicine (No. 1646). Prior to the collection of blood or CSF samples, all subjects gave written informed consent permitting the analysis of their samples for research purposes as part of their clinical care.

Subjects

Between April 2007 and February 2013, we enrolled 53 HAM/TSP patients according to the inclusion and exclusion criteria shown in Table 1, and divided them into two cohorts based on the chronological order of their doctor's visits: a 30-patient Training set and a 23-patient Test set. Demographics and clinical characteristics of the Training set and Test set are shown in Table 2 and Table 3, respectively. Between April 2007 and December 2009, we enrolled 22 HTLV-1-infected ACs as control subjects for blood analysis and eight HTLV-1-infected subjects (seven ACs, one patient with smoldering ATL) as control subjects for CSF analysis according to the inclusion and exclusion criteria shown in Table 1. These two groups were not mutually exclusive; some ACs donated both blood and CSF to this study. Demographics of control subjects as compared to the HAM/TSP patients are shown in Table S1.

Sample preparation

Blood and/or CSF samples were obtained within a one-hour window for each subject. Peripheral blood samples were collected in heparin-containing blood collection tubes and serum-separating tubes. Plasma and PBMCs were obtained from the former tubes and serum was obtained from the latter. PBMCs were isolated with standard procedures using Pancoll® density gradient centrifugation (density 1.077 g/mL; PAN-Biotech GmbH, Aidenbach, Germany). Plasma and serum samples were stored at −80°C until

Table 1. Inclusion and exclusion criteria for this study.

	HAM/TSP	Control for Blood	Control for CSF
Inclusion Criteria	Willing and able to give informed consent		
	HTLV-1 seropositive individuals conformed by CLEIA and Western blot		
	Diagnosed with HAM/TSP as defined by WHO criteria		Choose to provide CSF for the purposes of differential diagnosis
Exclusion Criteria	History of treatment with corticosteroids or other immunomodulating drugs (interferon, cyclosporin, methotrexate, etc.)		
	Diagnosed with an autoimmune disease or other chronic inflammatory disorder aside from HAM/TSP		
	Diagnosed with additional disease affecting gait disturbance (e.g. parkinsonism, rheumatoid arthritis, cervical spondylosis, brain infarction, etc.)		
	History of severe urinary infection, decubitus scars, pneumonia, deep venous thrombosis, or other condition potentially affecting disease course within the last four years	Diagnosed with HAM/TSP as defined by WHO criteria	
	Diagnosed with adult T-cell leukemia (ATL)		

CLEIA = chemiluminescent enzyme immunoassay.
doi:10.1371/journal.pntd.0002479.t001

use. CSF was collected in polypropylene tubes. A small amount of CSF was used for routine laboratory tests, which included total protein, cell count, and IgG level. The remaining CSF was aliquoted into cryotubes and stored at −80°C until undergoing further analysis. All tests in this study were performed on samples from these frozen stocks.

Measurement of blood candidate markers

The serum concentration of sIL-2R was determined using an ELISA (Cell Free N IL-2R; Kyowa Medex Ltd., Tokyo, Japan). HTLV-1 proviral load was measured using real-time PCR, following DNA extraction from PBMCs, as previously described [29–31]. Plasma levels of IL-1β, TNF-α, and IFN-γ were measured using a cytometric bead array (CBA) (BD Biosciences, Franklin Lakes, NJ USA), which was used according to the manufacturer's instructions. Plasma concentrations of CXCL9, CXCL10, CXCL11, and CCL5 were also measured using a CBA (BD Biosciences).

Measurement of CSF candidate markers

CSF cell count was determined using the Fuchs–Rosenthal chamber (Hausser Scientific Company, Horsham PA USA). Total protein and IgG levels in the CSF were measured using a pyrogallol red assay and a turbidimetric immunoassay, respectively. The anti-HTLV-1 antibody titer was determined using the gelatin particle agglutination test (Serodia-HTLV-1; Fujirebio, Tokyo, Japan). CSF concentration of sIL-2R was determined using an ELISA (Cell Free N IL-2R; Kyowa Medex). CSF neopterin level was measured using high-performance liquid chromatography. IFN-γ and six chemokines (CXCL9, CXCL10, CXCL11, CCL3, CCL4, and CCL5) were measured using a CBA (BD Biosciences). The CSF concentrations of three chemokines (CCL17, CCL20, and CCL22) and IL-17A were measured using commercially available ELISA kits (CCL17, CCL20, and CCL22: TECHNE/R&D Systems, Minneapolis, MN USA; IL-17A: Gen-Probe, San Diego, CA USA). All assays were conducted according to the respective manufacturers' instructions.

Table 2. Demographics and clinical characteristics of HAM/TSP patients (Training Set).

	Total	Stable HAM/TSP	Deteriorating HAM/TSP	
	n = 30	n = 14	n = 11	*p*-value*
Demographics				
Age, y**	58 [37–75]	54.5 [39–75]	62 [53–72]	0.0183†
Female sex	80.0%	64.3%	90.9%	0.1696‡
Clinical characteristics				
Age of onset, y**	48 [20–70]	33 [20–58]	57 [40–70]	0.0021†
Disease duration, y**	12.5 [1–33]	19 [7–33]	9 [1–13]	0.0021†
OMDS**	6 [2–11]	5 [2–9]	8 [5–11]	0.0065†

In the Training set, deteriorating patients were significantly older, experienced disease onset later in life, had been living with the disease for shorter periods, and were more severely disabled (OMDS).
*Stable HAM/TSP vs Deteriorating HAM/TSP.
**Data are expressed as median [range].
†By Mann-Whitney test.
‡By Fisher's exact test.
OMDS = Osame's Motor Disability Score.
doi:10.1371/journal.pntd.0002479.t002

Table 3. Demographics and clinical characteristics of HAM/TSP patients (Test Set).

	Total	Stable HAM/TSP	Deteriorating HAM/TSP	
	n = 23	n = 11	n = 9	*p*-value*
Demographics				
Age, y**	58 [22–75]	61 [22–75]	59 [48–68]	0.8491†
Female sex	78.3%	81.8%	77.8%	1.000‡
Clinical characteristics				
Age of onset, y**	43 [12–70]	40 [14–70]	51 [39–63]	0.0184†
Disease duration, y**	9 [2–41]	19 [5–41]	6 [2–14]	0.0148†
OMDS**	5 [2–8]	5 [4–8]	5 [4–8]	0.4526†

In the Test set, deteriorating patients experienced disease onset later in life and had been living with the disease for shorter periods, but there were no significant differences in current age or OMDS.
*Stable HAM/TSP vs Deteriorating HAM/TSP.
**Data are expressed as median [range].
†By Mann-Whitney test.
‡By Fisher's exact test.
OMDS = Osame's Motor Disability Score.
doi:10.1371/journal.pntd.0002479.t003

Classification system based on the natural history of HAM/TSP

The 53 total HAM/TSP patients without any history of HAM/TSP-targeting treatments were interviewed using a questionnaire (Figure S2) to determine the changes in Osame's Motor Disability Score (OMDS) over time (Figure S3). OMDS is a standardized neurological rating scale as a measure of disability [10] (Figure S1). Based on the changes in OMDS, "deteriorating cases" and "stable cases" were identified in both the Training set and Test set patient cohorts. Patients with deteriorating HAM/TSP were defined as those whose OMDS worsened ≥3 grades over four years and patients with stable HAM/TSP were defined as those whose OMDS remained unchanged or worsened 1 grade over four years. Patients whose OMDS worsened 2 grades over four years were excluded from the patient cohort in order to create a larger gap between the deteriorating and stable patient groups.

Statistical analysis

GraphPad Prism 5 (GraphPad Software, Inc., La Jolla, CA USA) was used to plot graphs and perform statistical analyses. Differences between the two subject groups were tested using the Mann-Whitney U-test. Receiver operating characteristic (ROC) analysis was performed to examine the sensitivity and specificity of individual biomarkers. For the ROC analyses, an area under the ROC curve (AUC) of 1.0 was used to represent a perfect test with 100% sensitivity and 100% specificity, whereas an area of 0.5 was used to represent random discrimination. Spearman's rank correlation test was employed to investigate the correlation between the four CSF markers (CXCL10, CXCL9, neopterin, and cell count) and the proviral load in PBMCs. To compare the four CSF markers between three groups (HTLV-1-infected control, n = 8; stable HAM/TSP, n = 25; and deteriorating HAM/TSP, n = 20), we used the Kruskal–Wallis test followed by Dunn's post-hoc tests. P-values<0.05 were considered statistically significant.

Results

Identification of biomarkers elevated in the blood of HAM/TSP patients

In order to identify candidate blood markers for HAM/TSP, the concentrations of IL-1β, TNF-α, and IFN-γ were measured in plasma samples from four ACs and four HAM/TSP patients. Plasma levels of IL-1β and TNFα were below the detection limits (<2.3 pg/mL and <1.2 pg/mL, respectively) except in one patient with HAM/TSP. Plasma IFN-γ levels showed no significant differences between ACs and HAM/TSP patients (median 10.4 pg/mL and 13.9 pg/mL, respectively). Therefore, these quantities were not measured in additional samples (Figure S1). The proviral DNA load in PBMCs, serum sIL-2R, and plasma levels of the chemokines CXCL9, CXCL10, CXCL11, and CCL5 were also measured in 22 ACs and 30 HAM/TSP patients without any history of immunomodulating treatments, including corticosteroids, IFN-α, and immunosuppressive drugs. The results revealed that serum levels of sIL-2R, plasma levels of CXCL10 and CXCL9, and proviral DNA load in PBMCs were markedly higher in HAM/TSP patients compared to ACs ($p \leq 0.0001$, Figure 1A). These quantities were then compared using ROC analysis to determine which parameters were superior markers for HAM/TSP. From the results of the ROC analysis, we determined that serum sIL-2R and plasma CXCL10 had the highest potential for distinguishing HAM/TSP patients from ACs with high sensitivity and specificity (area under the ROC curve [AUC]>0.9), followed by plasma CXCL9 and HTLV-1 proviral load in PBMCs (0.8<AUC<0.9) (Figure 1B). Thus, four candidate blood biomarkers were selected for further investigation: serum sIL-2R, plasma CXCL10, plasma CXCL9, and HTLV-1 proviral load in PBMCs.

Identification of biomarkers elevated in the CSF of HAM/TSP patients

In order to identify candidate CSF markers for HAM/TSP, elevated levels of various potential markers were screened for in CSF samples from HAM/TSP patients. CSF IL-17A was detectable (>3.0 pg/mL) in only one of eight HAM/TSP patients screened (including six deteriorating-type patients), and the level in this one patient (deteriorating-type) was negligible (4.0 pg/mL). CSF IFN-γ was detectable (>1.8 pg/mL) in only 3 of 10 HAM/TSP patients screened (six deteriorating patients), and the levels in all three were negligible (range 3.3–4.2 pg/mL). Therefore, these cytokines were not measured in additional patients. Total protein, cell count, IgG, neopterin, sIL-2R, and nine chemokines (CXCR3 ligands: CXCL9, CXCL10, and CXCL11; CCR5 ligands: CCL3, CCL4, and CCL5; CCR4 ligands: CCL17 and CCL22; CCR6